J. Membrane Biol. 145, 49–66 (1995)

The Journal of
Membrane
Biology

NO_3^- Transport Across the Plasma Membrane of *Arabidopsis thaliana* Root Hairs: Kinetic Control by pH and Membrane Voltage

A.A. Meharg*, M.R. Blatt
Department of Biological Sciences, University of London, Wye College, Wye, Kent TN25 5AH UK

Received: 4 October 1994/Revised: 21 December 1994

Abstract. High-affinity nitrate transport was examined in intact root hair cells of *Arabidopsis thaliana* using electrophysiological recordings to characterise the response of the plasma membrane to NO_3^- challenge and to quantify transport activity. The NO_3^--associated membrane current was determined using a three-electrode voltage clamp to bring membrane voltage under experimental control and to compensate for current dissipation along the longitudinal cell axis. Nitrate transport was evident in the roots of seedlings grown in the absence of a nitrogen source, but only 4–6 days postgermination. In 6-day-old seedlings, additions of 5-100 μM NO_3^- to the bathing medium resulted in membrane depolarizations of 8–43 mV, and membrane voltage (V_m) recovered on washing NO_3^- from the bath. Voltage clamp measurements carried out immediately before and following NO_3^- additions showed that the NO_3^--evoked depolarizations were the consequence of an inward-directed current that appeared across the entire range of accessible voltages (−300 to +50 mV). Both membrane depolarizations and NO_3^--evoked currents recorded at the free-running voltage displayed quasi-Michaelian kinetics, with apparent values for K_m of 23 ± 6 and 44 ± 11 μM, respectively and, for the current, a maximum of 5.1 ± 0.9 μA cm^{-2}. The NO_3^- current showed a pronounced voltage sensitivity within the normal physiological range between −250 and −100 mV, as could be demonstrated under voltage clamp, and increasing the bathing pH from 6.1 to 7.4–8.0 reduced the current and the associated membrane depolarizations 3- to 8-fold. Analyses showed a well-defined interaction between the kinetic variables of membrane voltage, pH_o and $[NO_3^-]_o$. At a constant pH_o of 6.1, depolarization from −250 to −150 mV resulted in an approximate 3-fold reduction in the maximum current but a 10% rise in the apparent affinity for NO_3^-. By contrast, the same depolarization effected an approximate 20% fall in the K_m for transport as a function in $[H^+]_o$. These, and additional characteristics of the transport current implicate a carrier cycle in which NO_3^- binding is kinetically isolated from the rate-limiting step of membrane charge transit, and they indicate a charge-coupling stoichiometry of 2(H^+) per NO_3^- anion transported across the membrane. The results concur with previous studies showing a high-affinity NO_3^- transport system in *Arabidopsis* that is inducible following a period of nitrogen-limiting growth, but they underline the importance of voltage as a kinetic factor controlling NO_3^- transport at the plant plasma membrane.

Key words: NO_3^--H^+ cotransport — *Arabidopsis thaliana* root hair cell — Plasma membrane — Transport, pH-dependent — Voltage clamp — Reaction kinetic model

Introduction

The capacity for active transport of NO_3^- is a feature common to higher plants, algae and fungi and plays an important role in maintaining the nitrogen status of the cell, notably under N-limiting conditions (Ullrich, 1987). The gross characteristics of these NO_3^- scavenging systems are similar among all walled eukaryotes: high-affinity NO_3^- transport is generally evident—or is greatly enhanced—following NO_3^- exposures (Schloemer & Garrett, 1974; Doddema et al., 1978; MacKown, 1987; Glass et al., 1990; Tischner et al., 1993) and exhibits often complex metabolite repression (Goldsmith et al., 1973; Doddema et al., 1978; Clarkson et al., 1989; Rufty,

* *Present address:* Institute of Terrestrial Ecology, Monks' Wood, Abbott's Ripton, Huntington, Cambs. PE17 2LS UK

Correspondence to: M.R. Blatt

Jr. et al., 1990; Henriksen & Spanswick, 1993; Tischner et al., 1993); the induction process, itself, is sensitive to inhibitors of protein synthesis (Schloemer & Garrett, 1974; Heimer & Filner, 1970); and once induced, transport exhibits an apparent affinity for NO_3^- typically in the range of 20–100 μM (Heimer & Filner, 1970; Schloemer & Garrett, 1974; Rao & Rains, 1976; MacKown, 1987; Ullrich, 1987; Goyal & Huffaker, 1986).

Compelling, if indirect evidence points to the coupling of high-affinity NO_3^- uptake with H^+, analogous to the H^+-cotransport systems of plants and fungi for inorganic anions (Beilby & Walker, 1981; Sanders & Hansen, 1981) and K^+ (Rodriguez-Navarro et al., 1986; Blatt & Slayman, 1987; Blatt et al., 1987), as well as for organic solutes such as sugars (Hansen & Slayman, 1978; Schwab & Komor, 1978; Bush, 1990) and amino acids (Sanders et al., 1983; McCutcheon & Bown, 1987; Li & Bush, 1990). Like the transport of these solutes, high-affinity uptake of NO_3^- can occur against its concentration gradient and membrane voltages that can exceed (–)200 mV (net electrochemical potential equivalent to a concentration gradient for the anion of 10^4–10^5) (Ullrich & Novacky, 1990; Ullrich & Novacky, 1981); NO_3^- uptake is sensitive to metabolic poisons and uncouplers (Heimer & Filner, 1970; Rao & Rains, 1976; Glass et al., 1990); in many species, including *Arabidopsis,* NO_3^- uptake is markedly pH dependent (Rao & Rains, 1976; Doddema & Telkamp, 1979; Fuggi, 1985; Ullrich and Novacky, 1990) and, where simultaneous measurements with net H^+ flux have been feasible, can be shown to entail roughly a stoichiometric (1:1) uptake of H^+ (Eddy & Hopkins, 1975); finally, NO_3^- transport is associated with membrane depolarization (Ullrich & Novacky, 1981; McClure et al., 1990; Ullrich & Novacky, 1990), indicating a movement of positive charge with NO_3^- across the plasma membrane. Thus, the overall consensus is of NO_3^- flux coupled to the movement of at least two H^+ with charge balance maintained by electrogenic H^+ extrusion via the H^+-ATPase of the plasma membrane.

The current situation, nonetheless, leaves as many questions unanswered. Electrophysiological studies, which have concentrated on changes in membrane voltage in response to extracellular NO_3^- additions, may not relate quantitatively to NO_3^- flux because displacements of membrane potential are subject to the background of other currents in the membrane (Blatt et al., 1987; Blatt, 1986; Sanders, 1990). Furthermore, voltage recordings have shown an often complex time course to the membrane depolarizations, including subsequent recoveries that occur over 5–15 min even in the presence of NO_3^- (Ullrich & Novacky, 1981; McClure et al., 1990). The situation is further complicated, since NO_3^--evoked depolarizations may be subject to the prevailing ionic conditions and extracellular pH. It has been argued that the "recovery" phase reflects activation of the H^+-ATPase (McClure et al., 1990) and that other inorganic ions may interact with the NO_3^- transporter (Ullrich et al., 1984; Ullrich & Novacky, 1990). Nonetheless, these observations must raise some doubt about the utility of such measurements when restricted to voltage deflections alone.

Fundamentally at issue is the kinetic contribution of the membrane potential itself. Implicit to transmembrane charge transport is the movement of charge across the membrane electrical field and, hence, a dependence on the membrane potential. Indeed, from a kinetic standpoint membrane potential is the electrical analogue of substrate concentration. Thus, membrane depolarization can limit uptake when the endogenous transport kinetics are sufficiently voltage sensitive (Blatt & Slayman, 1987; Blatt et al., 1987; McCulloch et al., 1990). This possibility alone might account for NO_3^- transport interactions with other ions, metabolites and pH which may, themselves, influence the membrane potential (Ullrich et al., 1984; Deane-Drummond, 1985; Henriksen et al., 1990).

To address these questions necessitates the use of voltage clamp techniques to bring membrane voltage under experimental control and to quantify the membrane current associated with NO_3^- transport. Yet, in work with higher plants, the difficulty of this approach lies in its requirement for a well-defined cell (or, more precisely, "electrical") geometry. With few exceptions, quantitative analyses of ATP-dependent and ion-coupled transport have been limited to simple, tractable cell preparations, notably the giant algae and the fungus *Neurospora.* For work with higher plants, the root hair offers one alternative, and a previous study demonstrated the feasibility of voltage clamp measurements using root hairs from intact roots of young *Arabidopsis* seedlings (Meharg et al., 1994). The present paper extends this work to explore the voltage-dependent characteristics of NO_3^- transport in *Arabidopsis* root hairs. The data show that NO_3^- uptake occurs in concert with the movement of positive charge across the membrane and indicate a charge-coupling stoichiometry of $2(+):1NO_3^-$. They demonstrate a pronounced voltage dependence to the transport current. Finally, the results show that external pH acts on the inherent kinetics for transport independent of any effects on the free-running membrane potential and consistent with transport coupling to H^+.

Material and Methods

Plant Growth and Experimental Protocol

Seedlings of *A. thaliana* L. cv. Landberg erecta were grown from seed affixed to lengths of glass coverslips with a pressure-sensitive, silicone medical adhesive (no. 355, Dow Corning, Midland, MI). The coverslips were placed in a minimal salts solution containing 5 mM Ca^{2+}-

MES/K^+-MES (5 mM 2-[*N*-morpholino]ethane sulfonic acid titrated to pH 6.1 with $Ca(OH)_2$, final $[Ca^{2+}] \approx 1$ mM, plus 0.2 mM of the same buffer titrated to pH 6.1 with KOH, final $[K^+] \approx 0.1$ mM) and the seeds allowed to germinate under a controlled environment of 25°C with a 16:8 hr day:night cycle. The coverslips were placed at an angle and immersed in Ca^{2+}-MES/K^+-MES buffer sufficient to wet the seed, but so that evaporation would draw the surface of the solution down the coverslip and avoid submerging the young roots.

For experiments, coverslips were transferred directly to the base of a chamber, open on two sides with a coverglass top (Meharg et al., 1994; Blatt, 1991), thus avoiding any disturbance to the young roots. The chamber was filled with Ca^{2+}-MES/K^+-MES buffer. Manipulations were observed under brightfield using a Leitz Orthopan microscope (Leitz, Wetzlar) fitted with 10× and 40× long-working distance objectives. Root hair dimensions and electrode placements were determined using a calibrated eyepiece micrometer. Measurements were carried out as described previously (Meharg et al., 1994) under fast solution flow (10 ml/min, ~20 chamber volumes/min) using a gravity feed and spent solution was removed by aspiration. The Ca^{2+}-MES/K^+-MES solution was used as the standard test buffer for experiments at pH_o 6.1. For measurements at pH_o 7.4 and 8.0, MES was replaced with HEPES (pK_a 7.4) and HEPPS (pK_a 8.0) titrated to their respective pK_as as before. Nitrate was added, as required, either as $NaNO_3$ or KNO_3.

Microelectrodes

Recordings were obtained using a three-electrode method by combining impalements with single- and double-barrelled microelectrodes (Blatt, 1991; Meharg et al., 1994). One impalement, with a double-barrelled microelectrode, was used to record voltage and pass current and a second impalement, with a separate single-barrelled microelectrode, was used to record voltage at a distance of 100–200 μm, either near the base of the cell or toward its tip. Current-passing and voltage-recording barrels/electrodes were filled with 100 mM K^+-acetate, pH 7.5, to minimize salt leakage and salt-loading artifacts associated with the Cl^- anion (Blatt & Slayman, 1983; Blatt, 1987*a*) without imposing a significant acid or alkaline load (Blatt & Armstrong, 1993), and microelectrodes were coated with paraffin to reduce electrode capacitance. Connection to the amplifier headstage was via a 1 M KCl/Ag-AgCl halfcell, and a matching halfcell and 1 M KCL-2% agar bridge served as the reference (bath) electrode.

Electrical

Mechanical, electrical and software design have been described in detail (Blatt, 1987*b;* Blatt, 1991; Meharg et al., 1994). Free-running membrane voltages were recorded on a Kipp-Zonen 1202 2-pen strip chart recorder (Metrabyte, Berks.). Current-voltage (*I-V*) relations were determined by the three-electrode method with the voltage clamp under microprocessor control using a WyeScience μP amplifier and μLAB analog/digital interface and software (WyeScience, Wye, Kent). Steady-state *I-V* relations were recorded by clamping cells to a bipolar staircase of command voltages (Blatt, 1987*b*). Steps alternated positive and negative from the free-running membrane potential, V_m (typically 20 bipolar pulse-pairs) and were separated by equivalent periods when the membrane was clamped to V_m. The current signal was filtered by a 6-pole Butterworth filter at 1 kHz (–3dB) before sampling, and currents and voltages were recorded during the final 10 msec of each pulse. The clamp comparator utilized the voltage recorded at the point of current injection (δV_0); voltage deflections at the second microelectrode (δV_1) were used to determine the space constant (λ) of the root hair and obtain I_m, the membrane current corrected for axial current dissipation, these calculations being carried out automatically under software control (WyeScience). The space constant and membrane current were determined by a linear cable approximation, where

$$\lambda = x \cdot \ln(\delta V_0/\delta V_1) \text{ and} \quad (1)$$

$$I_m = I_0 \cdot \ln(\delta V_0/\delta V_1)/\pi x, \quad (2)$$

where x is the distance between microelectrodes, I_0 is the (uncorrected) clamp current, and π has its usual meaning. No attempt was made to compensate for the series resistance (R_S) to ground (Hodgkin et al., 1952). Estimates for R_S indicated that it was unlikely to pose a serious problem in measurements of clamp potential.

Numerical Analysis

Data analysis was carried out by nonlinear, least-squares (Marquardt, 1963) and, where appropriate, results are reported as the mean ± SE of (n) observations. Difference-current-voltage (δI-V) curves were derived by subtracting whole-membrane *I-V* relations after polynomial fitting as described in the Results. Current-voltage characteristics and stoichiometries for NO_3^- transport were determined by fitting families of δI-V curves (obtained over a range of $[NO_3^-]_o$) to an explicit reaction-kinetic carrier model (Eq. 4, *see* Results). The number of free parameters was minimised by holding all but two or three in common. Otherwise, the relevant parameter products were constrained between curves to ratios (±50%) consistent with the differences in $[NO_3^-]_o$ and giving a maximum of two free parameters per δI-V curve. Fittings were carried out using modified Marquardt-Levenberg or Simplex algorithms (Press et al., 1986; Marquardt, 1963; Nelder & Mead, 1965). Simplex approach is highly opportunistic, but robust so long as the initial parameter estimates are nondegenerate. As a check against early convergence or local minima, fittings were routinely restarted at least three and occasionally 4–6 times—with secondary estimates chosen randomly within a range 10^1- to 10^3-fold above and below the previously fitted value—until trials converged on a common set of parameters. For additional details on the model, *see* the Results.

Chemicals and Solutions

The pH buffers were from Sigma Chemical Co. (St. Louis, MO). Otherwise, all chemicals were Analytical Grade from BDH Ltd. (Poole, Dorset, UK). Solutions were made up in water freshly double-distilled over Pyrex glass.

Results

NO_3^- Transport Induction and its Effect on Membrane Voltage

Arabidopsis seedlings grown in Ca^{2+}-MES/K^+-MES buffer received no additional nitrogen beyond what was available from the seed reserve. Under these conditions plants could be maintained for 10–12 days from germination, with shoots developing the first true leaves and roots growing to lengths of 3–4 cm. Seedling growth was noticeably retarded after 7–8 days, by comparison with plants grown in the presence of added $NaNO_3$ or on a nutrient repleat (Hoagland's salts) medium (Salisbury

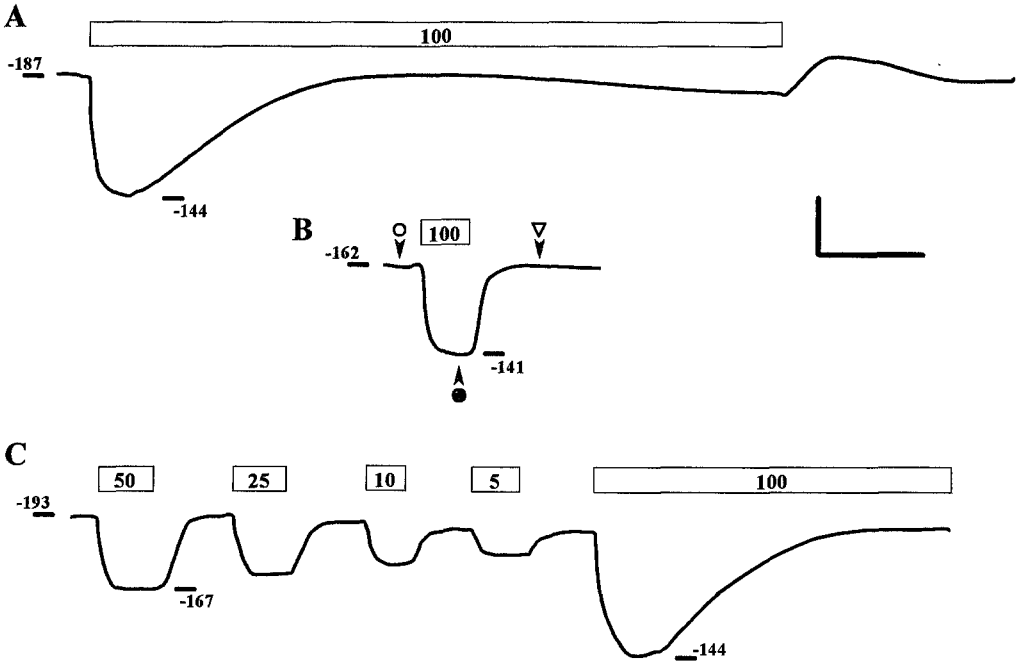

Fig. 1. Response of the free-running membrane potential of *Arabidopsis* root hair cells to NO_3^- exposures. Data from three separate experiments with cells bathed in Ca^{2+}-MES/K^+-MES, pH 6.1 and NO_3^- added as the Na^+ salt. Exposures to NO_3^- in μM concentrations indicated by the time bars above each trace. Voltages by the traces are in mV. Scale: 20 mV (vertical), 5 min (horizontal). Symbols and carats in trace B cross-reference with Fig. 3 and mark times of voltage-clamp scans (masked from trace) were run.

& Ross, 1984). The appearance of high-affinity transport activity for NO_3^- was monitored on successive days from day 3 after germination when the first root hairs were sufficiently developed for multiple impalements and voltage clamp studies. However no transport activity was evident, as could be ascertained by electrical recordings, before day 4 from germination and uniformly high activities were evident only by day 6 (*data not shown*). At this stage in growth, the *Arabidopsis* seedlings yielded a high density of root hairs often well in excess of 0.5 cm. Therefore, all subsequent experiments were carried out on 6-day-old seedlings.

For seedlings grown in the absence of added N, free-running membrane potentials (V_m) recorded in the Ca^{2+}-MES/K^+-MES buffer were -192 ± 12 ($n = 22$) and significantly more negative than those recorded from plants grown on N-replete media (Meharg et al., 1994). Nutrient starvation frequently augments free-running membrane potentials (Ullrich & Novacky, 1981; Rodriguez-Navarro et al., 1986; Blatt et al., 1987; Newman et al., 1987; Sanders, 1990), although in this instance the observation may not have been exclusively related to the N-depleted state of the root hairs. Adding NO_3^- to the medium bathing 6-day, but not 3-day (and frequently 4-day) old seedlings, evoked an immediate depolarization of the membrane, with measurable changes evident even in 5 μM NO_3^- (Fig. 1*C*). The voltage response was fully reversible provided that NO_3^- exposures were brief (Fig. 1*B,C*). However, prolonging exposures to NO_3^- for more than 2–3 min lead to a spontaneous recovery of the potential in the presence of NO_3^- (Fig. 1*A,C*), and subsequent washing of NO_3^- from the bath was marked by a secondary overshoot (negative-going) and recovery of V_m (Fig. 1*A*), in a manner characteristic of responses to NO_3^- in many tissues (Ullrich & Novacky, 1981; McClure et al., 1990). Comparable results were obtained in all 26 cells challenged with $NaNO_3$.

Voltage recordings such as the one shown in Fig. 1*C* indicated that the depolarizations initially evoked by NO_3^- described a hyperbolic function of the anion concentration. Because any current carried by a coupled NO_3^- transporter should saturate as the NO_3^- concentration becomes nonlimiting, the associated voltage displacements might also be expected to show quasi-Michaelian behavior. The data in Fig. 2 confirm this expectation: a plot of voltage changes recorded from cells exposed to a range of NO_3^- concentrations showed that the depolarizations were well-fitted with an apparent K_m of 23 ± 6 μM, comparable with values obtained from *Lemna* (Ullrich & Novacky, 1981) and *Zea* (McClure et al., 1990), and in NO_3^- uptake measurements from *Arabidopsis* (Doddema & Telkamp, 1979), wheat (Goyal & Huffaker, 1986), barley (Rao & Rains, 1976) and tobacco (Heimer & Filner, 1970).

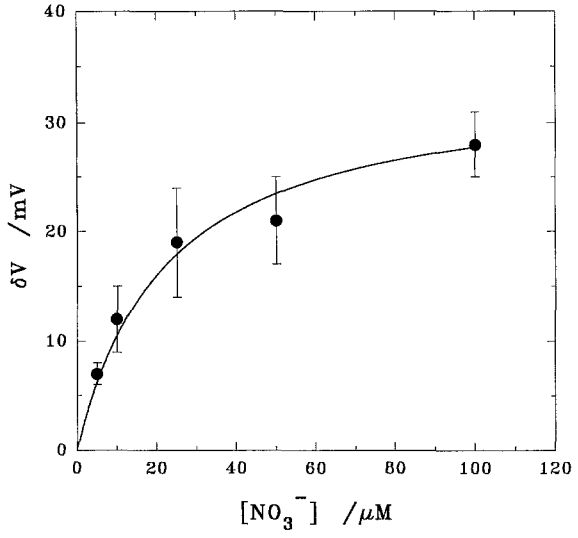

Fig. 2. Membrane depolarization in *Arabidopsis* root hair cells evoked by NO_3^- as a function of NO_3^- concentration in the bath. Steady-state voltage changes recorded in the first 2 min exposure to NO_3^- (*see* Fig. 1). Data points were pooled from 22 cells and are shown as means ± SE. The continuous curve is the result of nonlinear least-squares fitting to a hyperbolic tangent (Michaelis) function. Fitting parameters: K_m, 23 ± 6 μM; δV_{max}, 34 ± 4 mV.

Voltage-dependent Characteristics of the NO_3^--Evoked Current

One difficulty with analyses such as illustrated in Fig. 2 is that it ignores any possible voltage dependence to the overall membrane conductance or to the NO_3^--evoked current itself. Membrane depolarization inevitably reflects the balance of current, in this case through NO_3^--dependent and NO_3^--independent pathways. So, on the basis of voltage measurements alone, the transport system might seem to approach substrate saturation if depolarizations placed the membrane in a voltage range of relative high background (NO_3^--independent) conductance. The membrane conductance of *Arabidopsis* root hairs can show an appreciable voltage dependence (Meharg et al., 1994). Thus, the membrane current characteristics underlying these depolarizations were examined under voltage clamp, both to check against such kinetic "distortion" and to establish the voltage dependence of the NO_3^--evoked current itself.

To this end, steady-state currents across the root hair membrane were recorded at voltages between −300 and +50 mV and at intervals throughout these experiments before, during and after exposures to NO_3^-. In order to estimate the NO_3^--induced currents, independent of other transport functions at the root hair membrane, difference currents (δI) were calculated by subtracting the control *I-V* curve recorded before NO_3^- addition from the corresponding *I-V* curve determined in the presence of NO_3^-. Two assumptions underlie this technique: (i) the effects of substrate (in this case NO_3^-) addition should be limited primarily, if not exclusively, to the transport system being studied; and (ii) in the absence of substrate ($[NO_3^-]_o \cong 0$) current associated with forward operation of the transport system (NO_3^- uptake) should be everywhere zero.

These conditions were reasonably met here for short-term exposures to NO_3^-. In the absence of added NO_3^-, the major components of the control *I-V* relationship were well-accommodated by the characteristics for a H^+-ATPase with a charge stoichiometry of $1(H^+)$: 1(ATP) and a nonlinear leak, manifest as the rising outward current at strong depolarizations (R. Blatt and A. Meharg, *manuscript in preparation*). Furthermore, following brief exposures (<2 min) to NO_3^- the membrane *I-V* characteristics commonly recovered to the control state. The data in Fig. 3 and the corresponding voltage trace (Fig. 1*B*, cross-referenced by symbol) are typical. Membrane depolarization in NO_3^- was associated with a downward (negative-going) shift in the membrane *I-V* curve which was evident across the accessible voltage spectrum (Fig. 3*A*) and, on washing NO_3^- from the bath, both membrane voltage (Fig. 1*B*) and current (Fig. 3*A*) recovered. Thus, in toto the measurements accounted for the initial depolarization as the direct result of substrate (NO_3^-) addition and its consequence in engaging the endogenous kinetics for transport.

Figure 3 also shows qualitative changes to the membrane *I-V* characteristic in NO_3^-. Notably, NO_3^- addition increased membrane conductance at voltages negative of −100 mV but had little effect or even reduced the overall membrane conductance at voltages near and positive of this value. The effect is characteristic of an evoked, voltage-dependent current, and this expectation was confirmed by current subtraction. The difference current evoked by NO_3^- is indicated by the shading (Fig. 3*A*) and the resulting δI-*V* relation is plotted in Fig. 3*B*. In this particular trial, the current decreased in magnitude from approx. (−)18 μA cm^{-2} at −300 mV to a minimum of 2.6 μA cm^{-2} around −50 mV. Comparable results were obtained in all 18 cells subjected to voltage clamp analysis (*see also* Fig. 4), with a mean current of 7.8 ± 1.4 μA cm^{-2} at a common voltage of −200 mV when bathed in 100 μM NO_3^- and Ca^{2+}-MES/K^+-MES buffer at pH 6.1.

Remarkably, in every case NO_3^- additions yielded δI-*V* curves showing an appreciable *increase* in inward-directed current—and an apparent negative slope to the curve—at potentials positive-going from −100 mV to +50 mV (*see* Fig. 3*B*). This behavior stands out against the anticipated situation for transport equilibrium, since the current would be expected to *cross* the voltage axis around +20 mV for a cell bathed in 100 μM NO_3^- at pH 6.1, assuming an approximate internal pH of 7.5, $[NO_3^-]_i \cong 1$ mM (Miller & Zhen, 1991; Zhen et al., 1991) and a

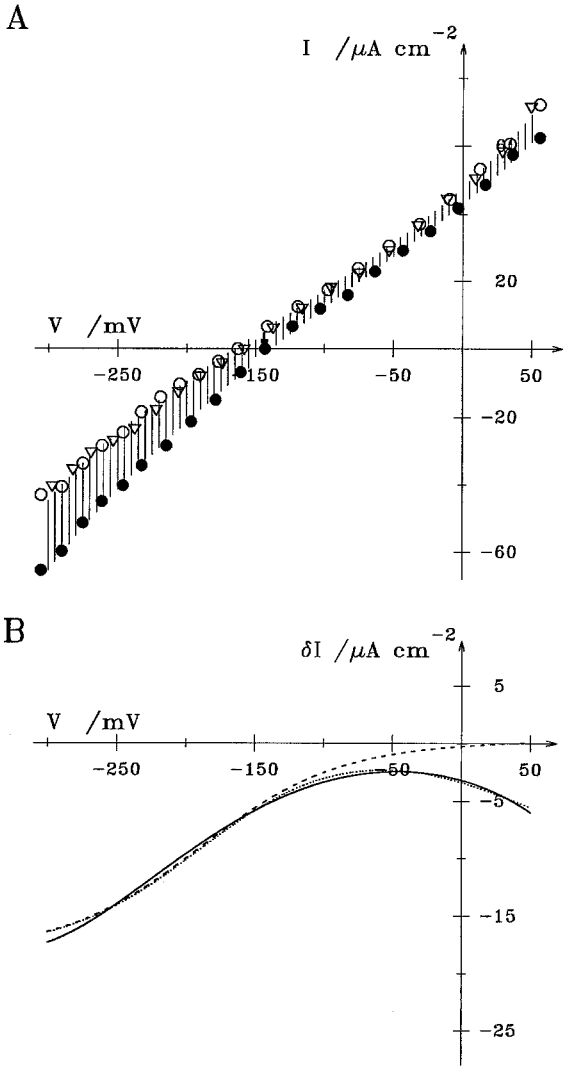

Fig. 3. Steady-state current-voltage (*I-V*) and difference-current-voltage (δI-*V*) curves obtained from one *Arabidopsis* root hair cell. (A) *I-V* curves determined at time points before (○), during (●) and after (▽) exposure to 100 μM NO_3^-. Vertical shading corresponds to the δI-*V* curve in B, and the voltage trace for the recordings is shown in Fig. 1*B*. The arrow (V_m in NO_3^-) indicates the NO_3^- difference current at the free-running potential in NO_3^-. (B) The δI-*V* curve derived by subtracting currents recorded before, from those recorded during NO_3^- exposure (continuous curve). Note the different current scale from *A*. The dotted and dashed curves are the results of nonlinear least-squares fitting of the data to Eq. 6 as detailed in the text. The dotted curve indicates the fitted δI-*V* characteristic; the broken curve is the predicted (true) *I-V* characteristic for the transporter. Fitting parameters with 100 μM NO_3^- (in s^{-1}): k^o_{oi}, 0.42; k^o_{oi}, 4.55; k_{io}, 0.53; k_{oi}, 18.2; E_{rev}, +28 mV. The first two parameters were held in common $\pm NO_3^-$; z was held to a value of −1.

coupling to $2H^+$. It is, nonetheless, a predictable consequence of current subtraction and arises simply because the experimental manipulations (NO_3^- addition/withdrawal) themselves affect the thermodynamic constraints on transport (Blatt, 1986). Cytoplasmic concentrations

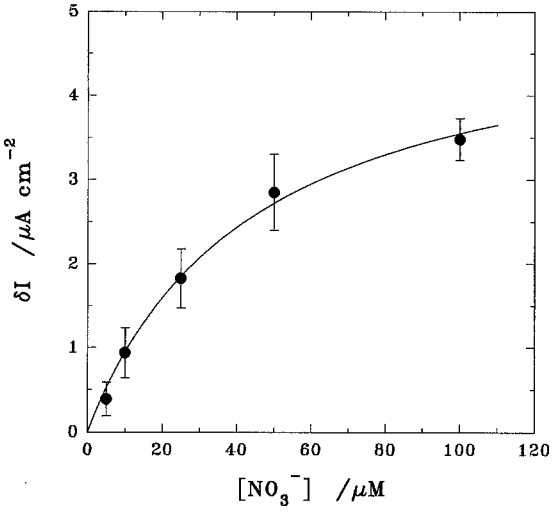

Fig. 4. Nitrate transport current at the free-running membrane potential in *Arabidopsis* root hair cells as a function of NO_3^- concentration in the bath. Currents pooled from 15 cells, determined as the difference between *I-V* curves calculated at the free-running potential in NO_3^- (*see* arrow, Fig. 3). Data shown are means ± SE. The solid curve is the result of nonlinear least-squares fitting to a hyperbolic tangent (Michaelis) function. Fitting parameters: K_m, 44 ± 13 μM; δI_{max}, 5.1 ± 0.8 μA cm^{-2}.

of both substrate and putative driver ion can be assumed to have been appreciable at all times in these experiments, and driving the membrane to extreme positive voltages would, thus, produce a current through the transport system *even when extracellular NO_3^- was zero.* In other words, in this voltage range both the control and test *I-V* curves must contain a component of NO_3^- transport current. So, simple *I-V* subtraction will give negative currents and negative slopes in this voltage range (Blatt, 1986). Fortunately, for practical purposes the δI-*V* data in the present experiments contain negligible subtraction error at voltages near and negative of −100 mV. Detailed fittings can be obtained over a wider voltage range by explicit use of the difference current equations (*see* Discussion and Blatt, 1986) to estimate the true current positive of −100 mV, and this is indicated by the dashed line in Fig. 3*B*. We return to the significance of these δI-*V* curves in the Discussion.

Kinetic Interaction of NO_3^-, pH_o and V_m

Data such as shown in Fig. 3 can be related directly to more conventional flux measurements of net (chemical) ion uptake, which are necessarily carried out without control of the membrane voltage. In this case, comparison must be based on difference currents calculated at the free-running potential (V_m) in the presence of NO_3^-. The relevant current is indicated by the arrow for the data in Fig. 3*A* and a summary of the results for measurements carried out at a constant pH_o 6.1 are shown in Fig.

4. Kinetic analysis of the pooled currents at pH_o 6.1 yielded an apparent δI_{max} of 5.1 ± 0.8 μA cm^{-2} and K_m of 44 ± 13 μM. The latter value points to a somewhat lower affinity for NO_3^- than indicated by the depolarization analysis (above) but offers a more satisfactory description of the transporter, being stoichiometrically related to the true chemical flux.

The Michaelis parameters above are a starting point for comparative analyses, but do not extend our understanding of NO_3^- transport in themselves. Because free-running membrane potentials in the N-starved root hair cells range between approx. −250 and −100 mV, measurements of NO_3^- transport will inevitably be subject to the kinetic variables of $[NO_3^-]_o$, $[NO_3^-]_i$, V_m, and assuming cotransport with H^+, also $[H^+]_o$ and $[H^+]_i$. In most transport experiments only two of these variables, $[NO_3^-]_o$ and $[H^+]_o$ are controlled directly. The cytoplasmic chemical concentrations may be considered constant in short term (initial rate) assays. However, V_m in most instances is wholly uncontrolled. Analyses such as illustrated in Fig. 3, make clear the effect of V_m on the NO_3^--evoked current within the normal range of free-running potentials. So, without explicit knowledge of the concomitant voltage changes, a comprehensive understanding is not possible for the behaviour of high-affinity NO_3^- transport, its dependence on substrate or its interaction with other (competing) transport activities at the plasma membrane.

To take account of the electrical variable, difference-current analyses were carried out as illustrated in Fig. 3 over a range of NO_3^- concentrations and at external pH values 6.1, 7.4 and 8.0. Analyses were generally restricted, however, to comparing currents recorded from the same cell in order to accommodate variations in current magnitudes between measurements (up to 2-fold on a cell-by-cell basis). Also, because of difficulties in maintaining stable recordings at the more alkaline pH values and over longer times, the measurements were limited to challenge with 100 μM NO_3^- at the two additional $[H^+]_o$. The currents recorded from one root hair challenged with 5–100 μM NO_3^- at pH_o 6.1 are shown in Fig. 5, and a comparable set of measurements carried out with a constant $[NO_3^-]_o$ over the three pH_o values is shown in Fig. 6. The δI-V curves are included in Fig. 5*B* and cross-referenced to Fig. 5*A* by symbol. Qualitatively comparable results were obtained in all experiments, and when the sequence of NO_3^- additions was reversed. Analogous results were also obtained in three cells challenged with 1 mM NO_3^-, although at this higher concentration δI-V curves were flattened (*data not shown*). Adding 100 μM NO_3^- resulted in the characteristic inward-going current, and exposures to lower concentrations of NO_3^- yielded analogous δI-V characteristics, albeit with smaller currents at any one voltage. Increasing $[NO_3^-]_o$ also had a qualitative effect on the δI-V curves, shifting the minimum in the current magnitude approximate 20

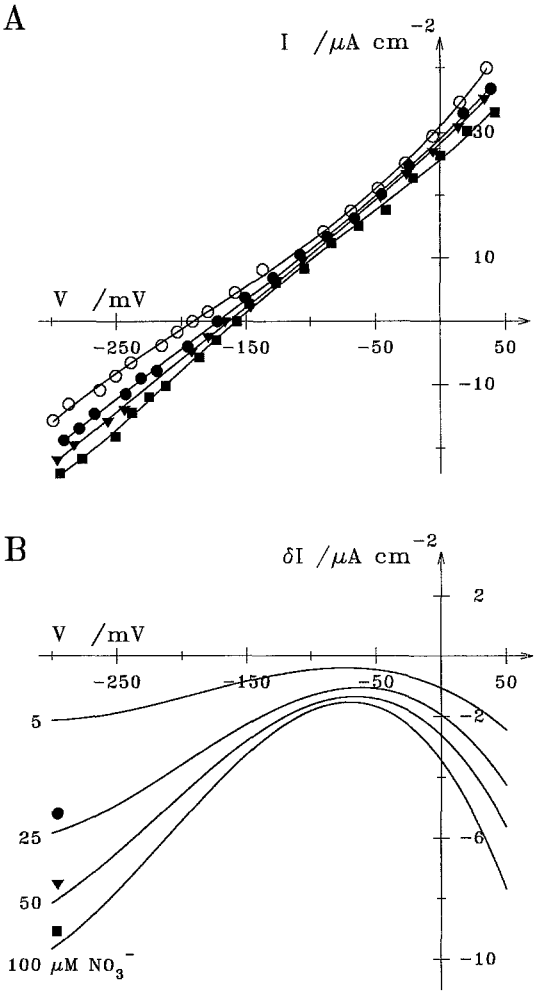

Fig. 5. Steady-state current-voltage (*I-V*) and difference-current-voltage (δI-V) curves as a function of NO_3^- concentration in the bath. Data from one *Arabidopsis* root hair cell. (A) *I-V* curves determined at time points before (○) and during challenge with 25 μM (●), 50 μM (▼) and 100 μM (■) NO_3^-. (B) δI-V curves derived by subtracting currents recorded before, from those recorded during NO_3^- exposures (*see* Fig. 3), cross-referenced to (*A*) by symbol and including additional data for 5 μM NO_3^-. Note the different current scales.

mV to more negative voltages over this concentration range. Reducing $[H^+]_o$, likewise, affected the current *independent* of the membrane voltage—reducing the NO_3^--evoked current at any one clamp potential—but also affected the δI-V profile by shifting the minimum in the current magnitude to more positive voltages (Fig. 6).

To bring these observations into a quantitative context, it is necessary to consider each independent variable separately. The simplest result to describe is the NO_3^- current dependence on pH_o at a fixed potential and $[NO_3^-]_o$. The data in Fig. 7 are for a clamp voltage of −250 mV and in 100 μM NO_3^- outside, including data from Fig. 6. The figure was assembled with data from three cells (symbols) after normalizing currents to the values recorded at pH_o 6.1, and clearly shows that raising

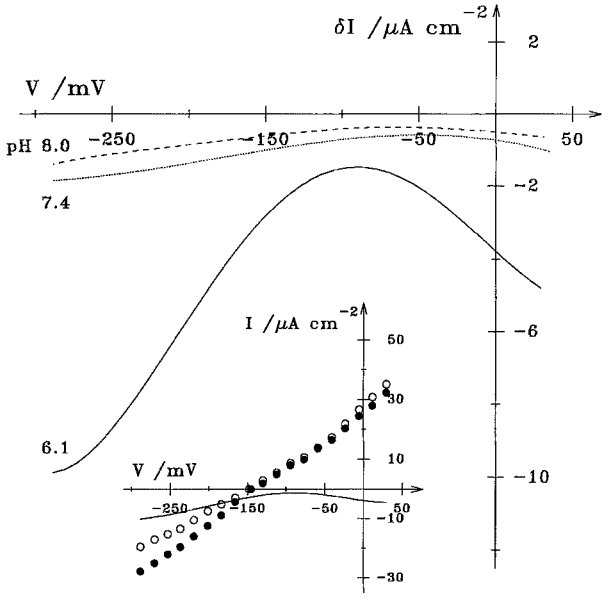

Fig. 6. Steady-state difference-current-voltage (δI-V) curves as a function of H^+ concentration in the bath. Data from one *Arabidopsis* root hair cell challenged with 100 μM NO_3^-. Curves are for NO_3^- exposures at pH_o 6.1 (continuous line), pH_o 7.4 (dotted line) and pH_o 8.0 (broken line). Inset: I-V data (○, $-NO_3^-$; ●, $+NO_3^-$) and δI-V curve for NO_3^- challenge at pH_o 6.1.

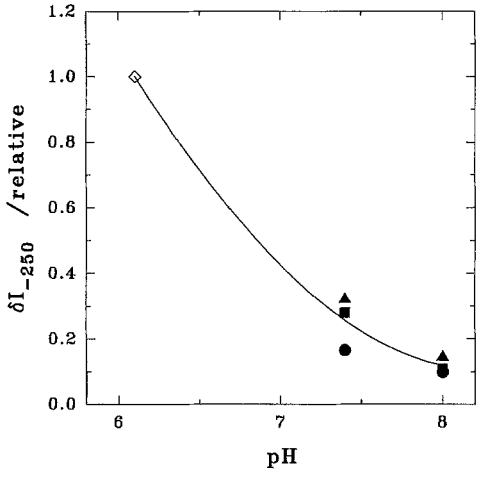

Fig. 7. Dependence of NO_3^- transport current on pH_o. Difference currents calculated for 100 μM NO_3^- exposures with the membrane clamped to −250 mV (*see* Fig. 3). Data are pooled from three experiments (symbols), with difference currents normalised to common measurements at pH_o 6.1 from each cell.

pH_o reduced the NO_3^--evoked current so that at pH_o 8.0 it was practically zero.

As noted above, the results in Fig. 6 also implicate an effect of $[H^+]_o$ on the inherent voltage dependence of the current, in that reducing $[H^+]_o$—increasing pH_o from 6.1 to 7.4–8.0—shifted the apparent δI minimum from about −100 mV to −50 mV. If we assume that H^+ con-

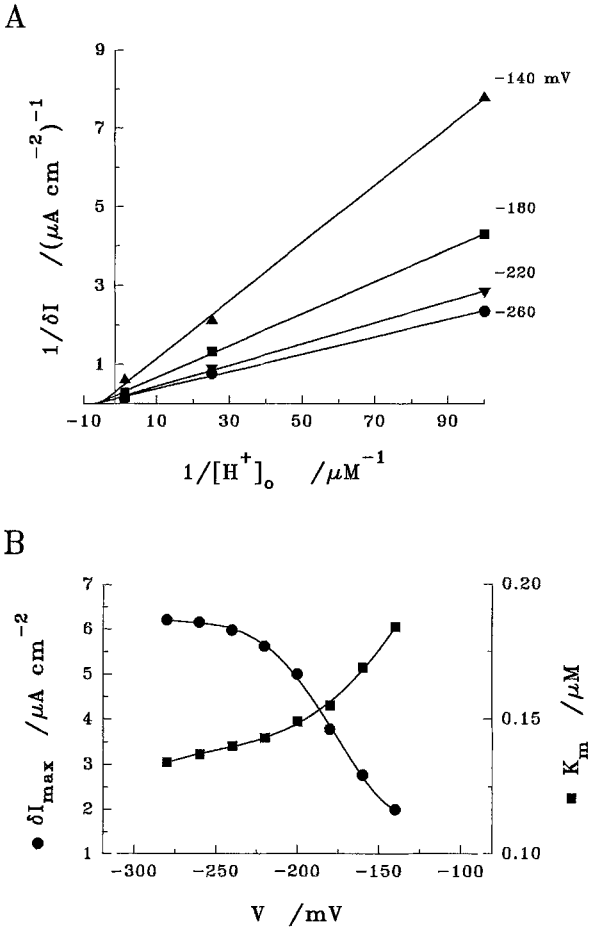

Fig. 8. Voltage-dependence of the kinetic parameters (δI_{max}, K_m) for the NO_3^- current, considered as a function of extracellular H^+ concentration. Methods as in Figs. 3 and 6, with data plotted for several membrane potentials and at near-saturating $[NO_3^-]_o$. A. Lineweaver-Burke plot of the data. Lines are from linear regression analyses of the data. (*B*) Plot of the kinetic parameters as a function of clamp voltage taken from (*A*).

tributes as a co-(driver-)ion for NO_3^- transport, a kinetically more meaningful view of this interaction can be obtained on transforming the data to derive the Michealis parameters for $[H^+]_o$ at each of several membrane voltages. Empirically best results were obtained treating the current as a function of $[H^+]_o$ rather than as a nonunitary power of the concentration[1], and Lineweaver-Burke plots for these data are shown in Fig. 8 along with the resulting values for K_m and δI_{max} at voltages between

[1] If, from the current voltage response associated with NO_3^- transport, we deduce that at least two H^+ are transported with the anion, then it might be anticipated that the current should follow a power function of $[H^+]$. That is, for 2 H^+ transport rate might depend on $([H^+]_o)^2$ (Segel, 1993). As will be seen from the kinetic considerations that follow (DISCUSSION), the current characteristics are entirely consistent with transport rate-limiting in only one of two H^+-binding steps.

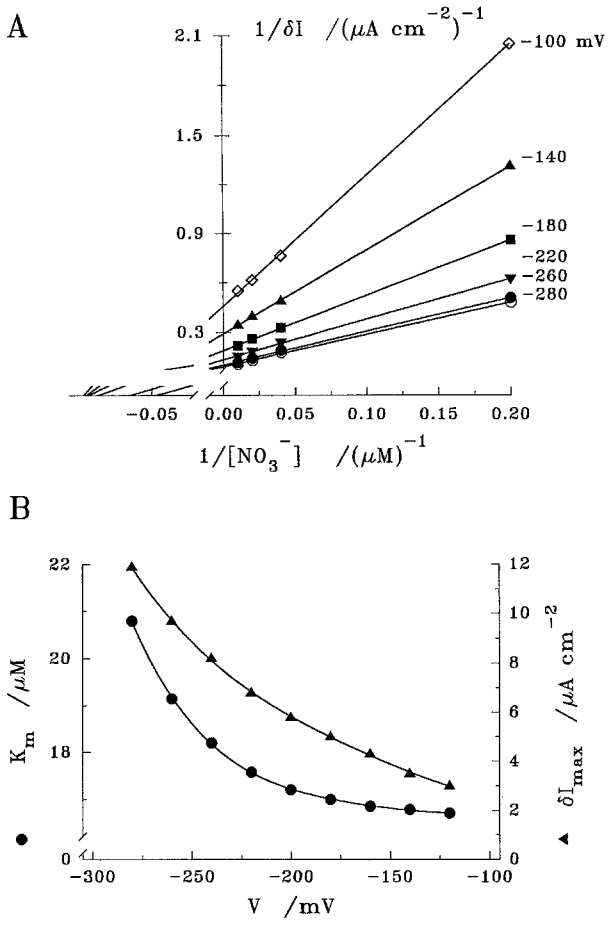

Fig. 9. Voltage-dependence of the kinetic parameters (δI_{max}, K_m) for the NO_3^- current, considered as a function of extracellular NO_3^- concentration. Methods as in Figs. 3 and 6, with data plotted for several membrane potentials and at pH_o 6.1. A. Lineweaver-Burke plot of the data. Lines are from linear regression analyses of the data. (B) Plot of the kinetic parameters as a function of clamp voltage taken from (*A*).

−280 and −140 mV. By analogy with inhibitors of ordinary enzymes (Segel, 1993), it is apparent that membrane voltage behaved as a "linear mixed-type activator" with respect to $[H^+]_o$: increasing (negative) voltage over this range lead to roughly a 3-fold rise in the maximum transport rate (current) and an approx. 20% increase in the apparent affinity for H^+.

Figure 9 summarizes the corresponding analysis carried out for NO_3^- as the substrate with pH_o held constant at 6.1. In this case, quite a different picture emerged, indicating that membrane voltage acted on δI_{max} and K_m *in parallel.* Again, by analogy with conventional enzyme kinetics (Segel, 1993), the behaviour was like a "hyperbolic mixed-type activator": both the maximal velocity of transport and the apparent K_m for NO_3^- increased together with (negative) voltage. This counter-intuitive observation suggested that NO_3^- binding should be kinetically remote from the charge transit step within the transport cycle, and we explore this point further in the Discussion below.

Discussion

It has generally been recognised that high-affinity NO_3^- uptake in higher plants and algae, as well as in fungi, is energetically unfavorable and requires that the cells of these tissues expend metabolic energy in the process. Membrane depolarizations have commonly been associated with NO_3^- uptake, pointing to a net *influx* of positive charge that must accompany the anion, and supporting the view that NO_3^- transport is coupled to the movement of at least two positive charges (H^+) into the cell. Along with the depolarizations recorded from *Arabidopsis* (Fig. 1), similar results have been described for NO_3^- transport in *Limnobium* (Ullrich & Novacky, 1990), *Lemna* (Ullrich & Novacky, 1981), *Zea mays* (McClure et al., 1990), and *Hordeum* (Glass et al., 1992) among other species.

By contrast, the implication of these depolarizations for the kinetics of NO_3^- transport has less often been appreciated. Our recordings underline the importance of the voltage parameter in assessing the characteristics for NO_3^- transport, its co-ion and—by inference—its metabolic, competing ion and inhibitor dependencies. Voltage clamp measurements exposed a significant sensitivity to voltage in the current (Figs. 3, 5, 6 and 9) while demonstrating an action of pH_o on the current *in*dependent of any change in membrane voltage (Figs. 6–8). This latter characteristic of the current and its insensitivity to other cations, notably Na^+, argues strongly in favour of a direct coupling of H^+ to drive NO_3^- uptake.

It is significant, too, that the voltage dependence of the NO_3^- current distinguishes it from the majority of currents previously identified in association with high-affinity transporters in plants or fungi. Proton-coupled transport of Cl^- (Beilby & Walker, 1981; Sanders & Hansen, 1981), amino acids (Schwab & Komor, 1978; Sanders et al., 1983; Felle, 1981) and sugars (Schwab & Komor, 1978), in large measure, have displayed only limited voltage sensitivities within the physiologically accessible voltage range. Instead, the characteristics for NO_3^- transport appear more closely allied to the K^+-H^+ symport of *Neurospora* (Blatt & Slayman, 1987; Blatt et al., 1987) and, at least superficially, to Na^+-K^+ currents in *Chara* (McCulloch et al., 1990). Thus, NO_3^- transport is significantly affected by the prevailing membrane potential within the relatively narrow range of voltages between −300 and −100 mV, and the current displays a minimum (conductance inflection) to the δI-V profile (Figs. 3, 5 and 6) at more positive-going voltages. Two questions arise, then: the first pertains to the charge stoichiometry and, hence, the coupling ratio of driver ions (H^+) transported with each NO_3^- anion; the second, and related issue concerns the nature of the kinetic interaction between NO_3^-, H^+ and the current.

A direct answer to the question of charge stoichiometry would entail comparing measured current equilibria with those predicted from a knowledge of the NO_3^- and H^+ concentrations on both sides of the membrane, or would require comparing chemical (radiotracer) flux and current under identical conditions. The latter option is not practicable for single cells in a complex tissue such as the higher-plant root, simply because of uncertainties about the relative contribution of the root hair population to macroscopic NO_3^- (chemical) uptake and because of the microscopic variability in transport current evident between root hairs (*see* Results). Likewise, the δI-V relations in this instance do not yield equilibrium potentials directly because the currents were derived by manipulating substrate concentrations. However, recognising the limitations of current subtraction, features of the δI-V curves nonetheless can provide important clues to the charge stoichiometry and to the underlying kinetic properties for NO_3^- transport.

Kinetic Dependence on Membrane Voltage and Charge Stoichiometry for NO_3^- Transport

Virtually all of the kinetic properties of the high-affinity NO_3^- transport current can be described by a few cyclic reaction models. To keep these models as simple and general as possible, no explicit physical assumptions need be made other than to propose that the transported ions traverse the membrane by reacting with a specific carrier molecule which is confined to the cell membrane. The models are conceived entirely in kinetic terms and may be reduced to the minimum number of pseudo first-order reaction steps that the experimental data will permit. No a priori assumption is made to identify rate-limiting reaction steps (Gradmann et al., 1987; Blatt et al., 1987). Finally, voltage dependence is introduced, following Läuger and Stark, [1970; *see also* Läuger, 1991], by assuming that transmembrane charge transit occurs in a single reaction step across a symmetric Eyring barrier according to the equations

$$k_{12} = k_{12}^{o} e^{zu/2} \quad [3a]$$

$$k_{21} = k_{21}^{o} e^{-zu/2} \quad [3b]$$

where $u = VF/RT$ and V is the membrane voltage; F, R and T have their usual meanings.

The minimal kinetic model that is physically consistent with a cotransport system for NO_3^- and two monovalent co-ions (H^+) comprises eight carrier states and fourteen rate constants which describe the sequential binding of substrate and co-ions on one side of the membrane and their debinding on the other side (*see* Fig. 10). Still higher coupling ratios entail correspondingly greater numbers of carrier states and co-ion (H^+) binding/debinding steps. The complete equation associated with any one of these cotransport models takes a general form where the transport current

$$I = -zF \frac{k_{12}|^1M_m| - k_{21}|^2M_m|}{|M_m|} \quad (4)$$

in which I is the current, m is the total number of states explicitly included in the model, $|M_m|$ is the determinant for the characteristic matrix of coefficients for that model, $|^jM_m|$ is the determinant for the adjusted matrix of coefficients excluding the jth state ($j = 1$ or 2, associated with membrane charge transit), the ratio $|^jM_m|/|M_m|$ is the total carrier in the jth state (N_1 or N_2), z is the charge moved per forward turnover of the carrier cycle, and F has its usual meaning.

From the standpoint of voltage clamp measurements, only the flux through the voltage-dependent transition is assayed directly; the remaining (electrically silent) reaction steps are indistinguishable from one another without additional information. So, for δI-V analyses, these may be subsumed within the single pair of pseudoreaction constants κ_{io} and κ_{oi}. Equation 4 then reduces to give

$$I - zFN \frac{k_{io}\kappa_{oi} - k_{oi}\kappa_{io}}{k_{io} + k_{oi} + \kappa_{io} + \kappa_{oi}} \quad (5)$$

where k_{io} and k_{io} are the pseudo-2-state equivalents of k_{12} and k_{21}, and N is a scalar relating the current to the total number of carriers in the membrane. Accordingly, the NO_3^--associated difference current

$$\begin{aligned}\delta I &= I_{+NO_3} - I_{-NO_3} \\ &= zFN\left[\frac{k'_{io}\kappa'_{oi} - k'_{io}\kappa'_{io}}{k'_{io} + k'_{oi} + \kappa'_{io} + \kappa'_{oi}}\right. \\ &\quad \left. - \frac{k_{io}\kappa_{oi} - k_{oi}\kappa_{io}}{k_{io} + k_{oi} + \kappa_{io} + \kappa_{oi}}\right]\end{aligned} \quad (6)$$

where the subscripts $+NO_3$ and prime constants refer to the transport current and reaction constants in the presence of external NO_3^-.

Two predictions fall immediately out of an analytical treatment of the steady-state carrier kinetics (Blatt, 1986). First, modifying carrier loading (e.g., by adding NO_3^-) will give a biphasic dependence of δI on voltage and negative slope (conductance) only when experimental manipulations affect a *rate-dominant* reaction step, that is when membrane charge transit is rate-limiting. In this case, the relative magnitudes of the charge-transit (k_{io}, k_{io}) and carrier recycling (κ_{io}, κ_{oi}) limbs of the reaction cycle can be indexed by the voltage span described by the slopes (positive-negative) of the δI-V relation. Second, δI-V curves will display—independent of the parent I-V relations—an axis of symmetry about

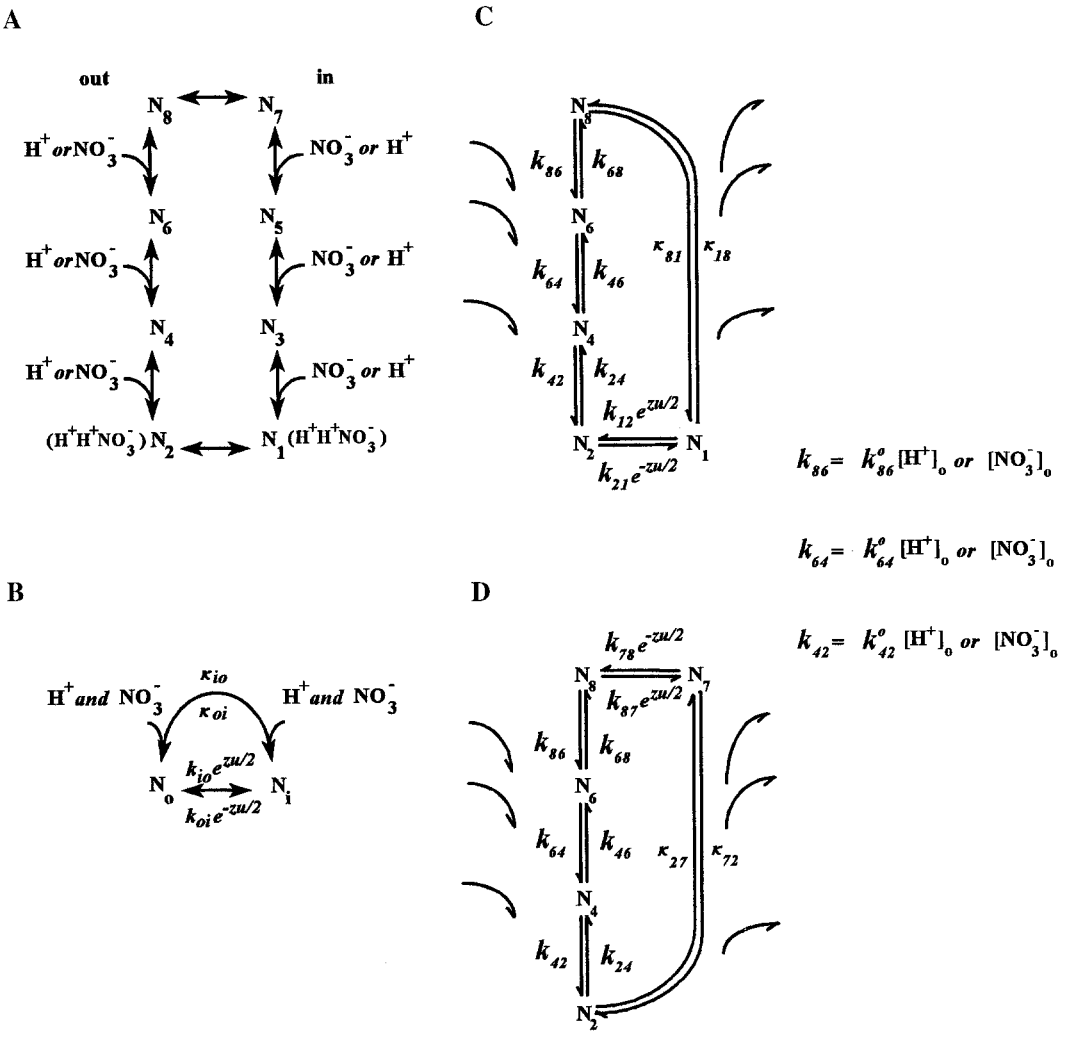

Fig. 10. Carrier cycle for the NO_3^- transporter. Forward operation in each case is in the counter-clockwise direction as illustrated. (A) The explicit, eight-state model with all possible binding/debinding orderings for H^+ and NO_3^- indicated. States N_1 and N_2 denote the loaded carrier states on the inside and outside of the membrane, respectively, while states N_7 and N_8 comprise recycling of the unloaded carrier across the membrane. All intervening steps entail binding/debinding of H^+ or NO_3^- inside and outside. (*B*) Pseudo-2-state reduction model equivalent. All binding/debinding steps and recycling of the uncharged carrier are subsumed in the lumped reaction constants κ_{io} and κ_{oi}. Membrane charge transit explicitly denoted by the reaction constants k^o_{io} and k^o_{oi}. The exponent factor z is the charge carried per cycle and the reduced membrane voltage $u = FV/RT$ where V is the membrane potential and F, R and T have their usual meanings. (*C*) Model I (*see* text): pseudo-5-state model equivalent with membrane charge transit assigned to the loaded carrier ($z = +1$). (D) Model II (*see* text): pseudo-5-state model equivalent with membrane charge transit assigned to the unloaded carrier ($z = -1$).

the equilibrium potential for the voltage sensitive limb of the reaction cycle

$$E_c = \frac{RT}{zF} \ln(k^o_{oi}/k^o_{io}) \qquad (7)$$

that coincides with the δI-V minima [conductance inflection; see also (Blatt et al., 1990)] such as evident in Figs. 3 and 5. Furthermore, these same characteristics can be called to account for the charge carried per reaction cycle when combined with additional information about proportional changes in one or more of the reaction steps, such as contained in a family of δI-V curves gathered over a series of defined substrate concentrations.

Now for NO_3^- transport, at least one additional driver ion must accompany the anion to account for the NO_3^--evoked current and membrane depolarizations; but higher coupling ratios with 2(+) charges (three driver ions) or more transported per NO_3^- are also possible. Selecting between plausible charge stoichiometries thus reduces to finding the best approximation of the pseudo-2-state model to families of δI-V curves by statistical minimization. To this end, numerical analyses were car-

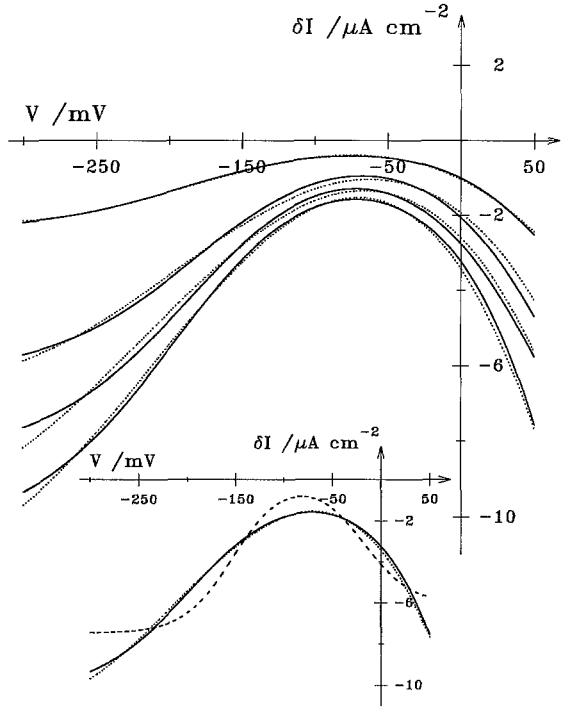

Fig. 11. *Arabidopsis* NO_3^- transport response to extracellular NO_3^- concentration. Nonlinear least-squares fitting of Eq. 6 to data of Fig. 5 shown as the solid curves. Dotted curves are the experimental δI-V relations. Joint fitting was carried out as described in the text, with k_{io}^o, k_{oi}^o, κ_{io} and κ_{oi} held in common between data sets, $k_{io}^{o\prime}$ constrained to equal k_{io}^o, and the remaining parameters constrained to give ratios of reaction constants consistent within a factor of 2 of the experimentally imposed changes in $[NO_3^-]_o$ [$E_{rev} = RT/zF \cdot ln(k_{oi}^o \kappa_{io}/k_{io}^o \kappa_{oi})$]. Parameter values held in common (s^{-1}): k_{io}^o, 0.21; k_{oi}^o, 5.45; κ_{io}, 12.98; κ_{oi}, $8.37 \cdot 10^{-6}$. Parameter values constrained in ratios (s^{-1}), 5 μM NO_3^-: $k_{oi}^{o\prime}$, 3.59; $\kappa_{io}^{\prime}$, 3.01; $\kappa_{oi}^{\prime}$, 2.22; 25 μM NO_3^-: $k_{oi}^{o\prime}$, 5.46; $\kappa_{io}^{\prime}$, 0.98; $\kappa_{oi}^{\prime}$, 5.97; 50 μM NO_3^-: $k_{oi}^{o\prime}$, 6.54; $\kappa_{io}^{\prime}$, 0.48; $\kappa_{oi}^{\prime}$, 8.51; 100 μM NO_3^-: $k_{io}^{o\prime}$, 8.19; $\kappa_{io}^{\prime}$, 0.20; $\kappa_{oi}^{\prime}$, 10.58. Predicted equilibrium potentials (E_{rev}, in mV) for 5, 25, 50 and 100 μM NO_3^-: −77, −36, −14, +7. These values are consistent with an intracellular NO_3^- concentration of approx. 1.5 mM [*see* also (Zhen et al., 1991; Miller & Zhen, 1991)]. Inset: Comparison of fittings for 100 μM NO_3^- with z constrained to −1 (continued curve) and −2 (broken curve). The dotted curve is the experimental δI-V relation.

ried out by least-squares, fitting families of δI-V curves jointly while constraining the charge factor z and all but one or a few of the reaction constants ($k_{io}^{\prime}$, $k_{oi}^{\prime}$, $\kappa_{io}^{\prime}$, $\kappa_{oi}^{\prime}$, k_{io}, k_{oi}, κ_{io} and κ_{oi}) to common values between δI-V curves. To accommodate the differences between experimental conditions as $[NO_3^-]_o$ was varied, the ratios of reaction constants associated with each NO_3^- treatment ($k_{io}^{\prime}$ $k_{oi}^{\prime}$, $\kappa_{io}^{\prime}$ and $\kappa_{oi}^{\prime}$) were constrained proportionally with respect to the reaction constants for the other curves. Numerical values, variable and joint, were then sought by sequential adjustments using Marquardt-Levenberg (Marquardt, 1963) or Simplex (Nelder & Mead, 1965) algorithms (see Material and Methods). Figure 11 shows the results of fittings to the δI-V curves shown in Fig. 5 and these are included in Table 1. Cor-

Table 1. Kinetic analysis of *Arabidopsis* NO_3^- transport δI-V relations

Parameter	Value
Fitted	
$k_{io}^{o\prime}/s^{-1}$	0.26 ± 0.08
$k_{oi}^{o\prime}/s^{-1}$	7.54 ± 0.82
$\kappa_{io}^{\prime}/s^{-1}$	0.14 ± 0.11
$\kappa_{io}^{\prime}/s^{-1}$	14.8 ± 3.1
Derived:	
E_{rev}/mV	31 ± 8
i_{-sat}/μA cm^{-2}	14.8 ± 3.1

Results are means ± SE of 4 sets of joint analyses for currents recorded with 5–100 μM NO_3^- as detailed in the text. Values shown are for 100 μM NO_3^-.

responding analyses are included with the data in Fig. 3. Satisfactory approximations to the experimental δI-V profiles with integer values for z were realized in every case only when z was constrained to a value of 1 (*see* Table 1). [The statistical treatment, in this case, does not of itself distinguish between models with charge carried by the loaded ($z = +1$) *vs.* unloaded carrier ($z = -1$), and equivalent fittings were obtained in each case. For reasons outlined below we have assigned the charge to the unloaded carrier.] The inset to Fig. 11 includes the best result obtained with z constrained to 2. Visually equivalent, but statistically better fittings were obtained when z was held in common between curves in any one family but otherwise allowed to vary freely. Even in these circumstances, however, values for z fell close to unity [0.96 ± 0.03 $n = 4$; range, 0.92–1.03]. In short, the characteristics of the NO_3^- δI-V profile accommodate quantitative description only with a single charge transported per carrier cycle with each NO_3^- ion.

Selecting a Minimal Reaction Scheme

Although the δI-V curve, of itself, relates directly only to the process of membrane charge transit, considerably more detail can be obtained when additional information ($[NO_3^-]$ and $[H^+]$) is taken into account. From the minimal kinetic model for $2H^+$-NO_3^- cotransport, two variants of this scheme may be considered, as diagrammed on the left in Fig. 10. Model I supposes the "carrier" molecule itself to be electrically neutral, so that the charges transported are the bound ions; model II accounts for the alternative case for which the unbound carrier molecule is charged (−1) and bears this charge across the membrane during carrier recycling. Taking account of substrate and co-ion binding order, each of these models actually comprises nine possible reaction sequences. However, because the experiments were not designed to manipulate $[NO_3^-]_i$ or pH_i—indeed, these parameters may be assumed constant—the data include little information about the (binding/debinding) reaction steps at

the inner surface of the membrane. So, the number of sequence permutations for each model can be reduced to three by lumping these steps with recycling of the uncharged carrier complex to give a pseudo-five-state model (Fig. 10, right-hand column). These reduced models follow the convention of Hansen et al. (1981), Sanders et al. (1984), Blatt (1986) and Gradmann et al. (1987) and are labeled accordingly: the k's designate simple reaction constants and the κ's designate the lumped constants that subsume multiple steps. Reaction constants which contain either voltage or ion-concentration terms are expanded at the far right in Fig. 10.

For Model I, membrane charge transit occurs in the transition $N_1 \rightleftharpoons N_2$, while in Model II charge movement occurs in the step between N_7 and N_8. Equation 4 holds in the latter case, because the steady-state assumption ensures that the net flux between N_7 and N_8 must equal that between N_1 and N_2. In either case, all of the matrices in Eq. 4 and its congeners represent linear combinations of the reaction constants. Many of the terms in the numerator cancel, but the general expression is non-Michaelian except under certain, well-defined circumstances, notably when the difference current δI, rather than the simple cotransport current, is calculated (Blatt, 1986; Blatt et al., 1987). Now the data presented in Figs. 8 and 9 describe sets of saturation (Michaelis) curves for which the maximal current (I_{max}) and Michaelis constant (K_m), determined as functions of substrate concentration $[NO_3^-]_o$ and $[H^+]_o$, are shown to be characteristic functions of the membrane voltage V_m. From a practical standpoint, the challenge thus is initially of identifying conditions which permit applying simplifying assumptions to the otherwise unwieldy Eq. 4.

The two limiting conditions that meet this criterion are of saturating negative membrane voltage and saturating substrate or co-ion concentration. Each of these conditions yields a simplified current equation with a single product term in the numerator and terms in the denominator which factor to give a sum of products in the substrate (or co-ion) concentration term and a second sum of products in a constant term. Thus Model I(L), that is with NO_3^- binding last before membrane charge transit, reduces to give:

$$\frac{I}{-FN} = \frac{k^\circ_{42}[NO_3^-]_o k^\circ_{21} e^{-u/2}\kappa_{18}}{k^\circ_{42}[NO_3^-]_o(k^\circ_{12}e^{u/2} + k^\circ_{21}e^{-u/2} + \kappa_{18}) + \kappa_{24}k^\circ_{12}e^{u/2} + \kappa_{18}k^\circ_{21}e^{-u/2}} \quad (8)$$

which, after minor rearrangement of terms, gives the Michaelis parameters

$$\frac{I_{max}}{-FN} = \frac{k^\circ_{21}e^{-u/2}\kappa_{18}}{k^\circ_{12}e^{u/2} + k^\circ_{21}e^{-u/2} + \kappa_{18}} \quad (9)$$

$$K_m = \frac{k^\circ_{12}e^{u/2}\kappa_{24} + k^\circ_{21}e^{-u/2}\kappa_{18}}{k^\circ_{12}e^{u/2} + k^\circ_{21}e^{-u/2} + \kappa_{18}} \quad (10)$$

Table 2 summarizes the Michaelis parameters for each of the two models in Fig. 10 and the six different orderings for substrate (NO_3^-) and co-ion (H^+) binding subsumed within them. The data address only conditions of saturating substrate and co-ion concentration, so Table 2 omits the third condition of saturating-negative membrane voltage. In every case, forward operation of the transporter, as depicted by the models (Fig. 10), occurs in the counter-clockwise direction. Note that for functions in $[H^+]_o$ the current equation is non-Michaelian, reflecting the compound dependence on H^+ binding, but becomes Michaelian in $[H^+]_o$ when the reaction constant for reverse (clockwise) transit through one of these steps is very small. We assume Michaelian behavior in these instances, and have included the "missing" reaction constants in the size orderings in each case below.

Identifying Competent Models

The problem of discriminating between the models in Fig. 10 reduces to one of finding a single set of conditions, defined by the size ordering of reaction constants in Table 2, which are internally consistent and which satisfy the pattern of I_{max} and K_m behavior in Figs. 8 and 9. Examining Table 2 shows that both of the models in all binding order combinations will account for the data in Fig. 9. In every case, orderings of reaction constants can be found which give a parallel increase of I_{max} and K_m as functions in $[NO_3^-]$ with increasing (negative) membrane voltage. By contrast, for all but a few of the cases, *no* size ordering of reaction constants will yield, with increasing (negative) membrane voltage, a *decrease* in K_m as functions in $[H^+]$. Only Models I(M) and II(M)—with NO_3^- binding second-to-last before charge transfer across the membrane—and Model II(L) give combinations of reaction constants for which K_m will decrease with (negative) membrane voltage consistent with Fig. 8.

Of these three, Models I(M) and II(L) entail inconsistencies in the ordering of reaction constants. To accommodate the voltage-dependence of K_m in $[H^+]$ (Fig. 8), Model II(L) requires that $\kappa_{72} \gg \kappa_{27}$, $k^\circ_{78}e^{-u/2}$, $k^\circ_{87}e^{u/2}$, $k^\circ_{86}[H^+]_o$, $k^\circ_{64}[H^+]_o \gg k_{68}$ (Table 2 column 4, row 18). However, this ordering conflicts with that required for K_m in $[NO_3^-]$ to increase with (negative) voltage (Table 2 column 2, row 17), and shows a weak inconsistency with the corresponding orderings for I_{max}, both in $[NO_3^-]$ and in $[H^+]$ (Table 2 columns 3 and 5, row 17). A similar set of conflicts is found in the ordering requirements for Model I(M) to accommodate the data. Only Model II(M) yields a single set of ordered reaction constants that are internally consistent and satisfy the data of Figs. 8 and 9. Taking account of all requirements gives the minimal overall ordering

$$\kappa_{72},\ k^\circ_{87}e^{u/2},\ k^\circ_{64}[NO_3^-]_o > k^\circ_{42}[H^+]_o,\ \kappa_{27} \gg k^\circ_{78}e^{-u/2},\ k^\circ_{86}[H^+]_o \gg k_{24} \quad [11]$$

Table 2. Summary of conditions for specified behaviors of K_m and I_{max} in $[NO_3^-]_o$ and $[H^+]_o$ when membrane voltage is varied.

Col:	1	2	3	4	5	
Function in:		NO_3^-(H^+ saturating)		H^+(NO_3^- saturating)		Row
model	Binding order	K_m	I_{max}/-FN	K_m	I_{max}/-FN	
I(F)	$S^-D^+D^+$	$\frac{k_{12}^o e^{u/2}\kappa_{81} + k_{21}^o e^{-u/2}(\kappa_{18}+\kappa_{81})}{k_{86}^o(k_{12}^o e^{u/2} + k_{21}^0 e^{-u/2} + \kappa_{18})}$	$\frac{k_{21}^o e^{-u/2}\kappa_{18}}{k_{12}^o e^{u/2} + k_{21}^o e^{-u/2} + \kappa_{18}}$	$\frac{k_{21}^o e^{-u/2}\kappa_{18}(k_{64}^o + k_{42}^o)}{k_{64}^o k_{42}^o(k_{12}^o e^{u/2} + k_{21}^o e^{-u/2} + \kappa_{18})}$	$\frac{k_{21}^o e^{-u/2}\kappa_{18}}{k_{12}^o e^{u/2} + k_{21}^o e^{-u/2} + \kappa_{18}}$	1
	⇑	$\kappa_{18} \gg \kappa_{81}, k_{12}^o, k_{21}^o$	$\kappa_{18} > k_{21}^o > k_{12}^o$ or $k_{12}^o \gg k_{21}^o, \kappa_{18}$	$k_{46}, k_{24} \simeq 0$ and $\kappa_{18} > k_{21}^o > k_{12}^o$ or $k_{12}^o \gg k_{21}^o, \kappa_{18}$	$k_{46}, k_{24} \simeq 0$ and $\kappa_{18} > k_{21}^o > k_{12}^o$ or $k_{12}^o \gg k_{21}^o, \kappa_{18}$	2
	⇓	~NC with $k_{21}^o, \kappa_{81} \gg \kappa_{18}$	~NC with $k_{21}^o \gg k_{12}^o, \kappa_{18}$	~NC with $k_{46}, k_{24} \simeq 0$ and $k_{21}^o \gg k_{12}^o, \kappa_{18}$	~NC with $k_{46}, k_{24} \simeq 0$ and $k_{21}^o \gg k_{12}^o, \kappa_{18}$	3
		$K_m \simeq 0$	$I_{max} \simeq 0$	$K_m \simeq 0$	$I_{max} \simeq 0$	
I(M)	$D^+S^-D^+$	$\frac{k_{21}^o e^{-u/2}\kappa_{18}}{k_{64}^o(k_{12}^o e^{u/2} + k_{21}^o e^{-u/2} + \kappa_{18})}$	$\frac{k_{21}^o e^{-u/2}\kappa_{18}}{k_{12}^o e^{u/2} + k_{21}^o e^{-u/2} + \kappa_{18}}$	$\frac{k_{21}^o e^{-u/2}\kappa_{18}(k_{86}^o + k_{42}^o) + (k_{12}^o e^{u/2} + k_{21}^o e^{-u/2})k_{42}^o\kappa_{81}}{k_{86}^o k_{42}^o(k_{12}^o e^{u/2} + k_{21}^o e^{-u/2} + \kappa_{18})}$	$\frac{k_{21}^o e^{-u/2}\kappa_{18}}{k_{12}^o e^{u/2} + k_{21}^o e^{-u/2} + \kappa_{18}}$	4
	⇑	$\kappa_{18} > k_{21}^o > k_{12}^o$ or $k_{12}^o \gg k_{21}^o, \kappa_{18}$	$\kappa_{18} > k_{21}^o > k_{12}^o$ or $k_{12}^o \gg k_{21}^o, \kappa_{18}$	$k_{68}, k_{24} \simeq 0$ and $\kappa_{81}, k_{12}^o \gg k_{21}^o$ or $\kappa_{18} > k_{21}^o \gg k_{42}^o, \kappa_{81}$	$k_{68}, k_{24} \simeq 0$ and $\kappa_{18} > k_{21}^o > k_{12}^o$ or $k_{12}^o \gg k_{21}^o, \kappa_{18}$	5
	⇓	~NC with $k_{21}^o \gg \kappa_{81}, \kappa_{18}$	~NC with $k_{21}^o \gg k_{12}^o, \kappa_{18}$	$\kappa_{81} > \kappa_{18} > k_{12}^o \gg k_{21}^o \gg k_{24}, k_{68}$	~NC with $k_{21}^o \gg \kappa_{81}, \kappa_{18} \gg k_{24}, k_{68}$	6
		$K_m \simeq 0$	$I_{max} \simeq 0$		$I_{max} \simeq 0$	
I(L)	$D^+D^+S^-$	$\frac{k_{12}^o e^{u/2} k_{24} + k_{21}^o e^{-u/2}\kappa_{18}}{k_{12}^o e^{u/2} + k_{21}^o e^{-u/2} + \kappa_{18}}$	$\frac{k_{21}^o e^{-u/2}\kappa_{18}}{k_{12}^o e^{u/2} + k_{21}^o e^{-u/2} + \kappa_{18}}$	$\frac{k_{21}^o e^{-u/2}\kappa_{18}(k_{86}^o + k_{64}^o) + (k_{12}^o e^{u/2} + k_{21}^o e^{-u/2})k_{64}^o\kappa_{81}}{k_{86}^o k_{64}^o(k_{12}^o e^{u/2} + k_{21}^o e^{-u/2} + \kappa_{18})}$	$\frac{k_{21}^o e^{-u/2}\kappa_{18}}{k_{12}^o e^{u/2} + k_{21}^o e^{-u/2} + \kappa_{18}}$	7
	⇑	$\kappa_{18} > k_{21}^o \gg k_{12}^o, k_{24}$ or $\kappa_{18} > k_{12}^o \gg k_{21}^o, k_{24}$	$\kappa_{18} > k_{21}^o > k_{12}^o$ or $k_{12}^o \gg k_{21}^o, \kappa_{18}$	$k_{68} \simeq 0$ and	$k_{68} \simeq 0$ and	8
				$\kappa_{81}, k_{12}^o \gg k_{21}^o, \kappa_{18}$ or $\kappa_{18} > k_{21}^o$ and $\kappa_{81} \sim 0$	$\kappa_{18} > k_{21}^o > k_{12}^o$ or $k_{12}^o \gg k_{21}^o, \kappa_{18}$ and $\kappa_{81} \sim 0$	
	⇓	$k_{21}^o, k_{24} \gg k_{12}^o, \kappa_{18}$	~NC with $k_{21}^o \gg k_{12}^o, \kappa_{18}$	~NC with $k_{68} \simeq 0$ and $\kappa_{18} \gg k_{12}^o, k_{21}^o, \kappa_{81}$	~NC with $k_{68} \simeq 0$ and $k_{21}^o \gg k_{12}^o, \kappa_{18}$	9

II(F)	$S^-D^+D^+$	$\frac{k^o_{78}e^{-u/2}(\kappa_{27}+k_{24})+\kappa_{72}k_{24}}{k^o_{42}(\kappa_{72}+\kappa_{27}+k^o_{78}e^{-u/2})}$	$\frac{k^o_{78}e^{-u/2}\kappa_{27}}{\kappa_{72}+\kappa_{27}+k^o_{78}e^{-u/2}}$	$\frac{k^o_{78}e^{-u/2}\kappa_{27}(k^o_{86}+k^o_{64})}{k^o_{86}k^o_{64}(\kappa_{72}+\kappa_{27}+k^o_{78}e^{-u/2})}$	$\frac{k^o_{78}e^{-u/2}\kappa_{27}}{\kappa_{72}+\kappa_{27}+k^o_{78}e^{-u/2}}$	10
	⇑	$\kappa_{27} > k^o_{78} \gg \kappa_{72},k_{24}$	$\kappa_{27} > k^o_{78},\kappa_{72}$ or $\kappa_{72} > k^o_{78}$	$k_{46} \simeq 0$ and $\kappa_{21} > k^o_{78},\kappa_{72}$ or $\kappa_{72} > k^o_{78}$	$k_{46} \simeq 0$ and $\kappa_{27} > k^o_{78},\kappa_{72}$ or $\kappa_{72} > k^o_{78}$	11
	⇓	$\kappa_{27} \gg \kappa_{72},k_{24}$	~NC with $k^o_{78} \gg \kappa_{72},\kappa_{27}$	~NC with $k_{46} \simeq 0$ and $k^o_{78} \gg \kappa_{72},\kappa_{27}$	~NC with $k_{46} \simeq 0$ and $k^o_{78} \gg \kappa_{72},\kappa_{27}$	12
			$I_{max} \simeq -FN\kappa_{27}$	$K_m \simeq \frac{\kappa_{27}(k^o_{86}+k^o_{64})}{k^o_{86}k^o_{64}}$	$I_{max} \simeq -FN\kappa_{27}$	
II(M)	$D^+S^-D^+$	$\frac{k^o_{78}e^{-u/2}\kappa_{27}}{k^o_{64}(\kappa_{72}+\kappa_{27}+k^o_{78}e^{-u/2})}$	$\frac{k^o_{78}e^{-u/2}}{\kappa_{72}+\kappa_{27}+k^o_{78}e^{-u/2}}$	$\frac{k^o_{42}(k^o_{87}e^{u/2}(\kappa_{72}+\kappa_{27})+k^o_{78}e^{-u/2})+(k^o_{86}(k^o_{78}e^{-u/2}(\kappa_{72}+\kappa_{24})+\kappa_{72}\kappa_{24})}{k^o_{86}k^o_{64}(\kappa_{72}+\kappa_{27}+k^o_{78}e^{-u/2})}$	$\frac{k^o_{78}e^{-u/2}\kappa_{27}}{\kappa_{72}+\kappa_{27}+k^o_{78}e^{-u/2}}$	13
	⇑	$\kappa_{27} > k^o_{78} > \kappa_{72},k_{24}$ or $\kappa_{72} > k^o_{78}$	$\kappa_{27} > k^o_{78},\kappa_{72}$ or $\kappa_{72} > k^o_{78}$	$k_{24} \simeq 0$ and $\kappa_{27} > k^o_{78} \gg \kappa_{12},k^o_{87}$	$k_{24} \simeq 0$ and $\kappa_{27} > k^o_{78},\kappa_{72}$ or $\kappa_{72} > k^o_{78}$	14
	⇓	~NC with $k^o_{78} \gg \kappa_{72},\kappa_{21}$ $K_m \simeq \frac{\kappa_{27}}{k^o_{64}}$	~NC with $k^o_{78} \gg \kappa_{72},\kappa_{27}$ $I_{max} \simeq -FN\kappa_{27}$	$k_{24} \simeq 0$ and k^o_{87},κ_{72}, $\kappa^o_{42} \gg \kappa_{27},k^o_{86},k^o_{78}$	~NC with $k_{24} \simeq 0$ and $k^o_{78} \gg \kappa_{72},\kappa_{27}$ $I_{max} \simeq -FN\kappa_{27}$	15
II(L)	$D^+D^+S^-$	$\frac{k^o_{78}e^{-u/2}(\kappa_{27}+k_{24})+\kappa_{72}k_{24}}{k^o_{42}(\kappa_{72}+\kappa_{27}+k^o_{78}e^{-u/2})}$	$\frac{k^o_{78}e^{-u/2}\kappa_{27}}{\kappa_{72}+\kappa_{27}+k^o_{78}e^{-u/2}}$	$\frac{k^o_{87}e^{u/2}k^o_{64}(\kappa_{12}+\kappa_{27})+k^o_{78}e^{-u/2}\kappa_{21}(k^o_{86}+k^o_{64})}{k^o_{86}k^o_{64}(\kappa_{72}+\kappa_{27}+k^o_{78}e^{-u/2})}$	$\frac{k^o_{78}e^{-u/2}\kappa_{27}}{\kappa_{72}+\kappa_{27}+k^o_{78}e^{-u/2}}$	16
	⇑	$\kappa_{27} > k^o_{78} \gg \kappa_{72},k_{24}$	$\kappa_{27} > k^o_{78},\kappa_{72}$ or $\kappa_{72} > k^o_{78}$	$k_{68} \simeq 0$ and $\kappa_{27} > k^o_{78} \gg k^o_{87},k^o_{64}$	$k_{68} \simeq 0$ and $\kappa_{27} > k^o_{18},\kappa_{72}$ or $\kappa_{72} > k^o_{18}$	17
	⇓	~NC with $k^o_{78} \gg \kappa_{72},\kappa_{27},k_{24}$ or $k_{24}\kappa_{72} \gg k^o_{78},\kappa_{27}$	~NC with $k^o_{78} \gg \kappa_{72},\kappa_{27}$ $I_{max} \simeq -FN\kappa_{27}$	$k_{68} \simeq 0$ and $\kappa_{72} \gg k^o_{78},k^o_{87},k^o_{86},k^o_{64},\kappa_{27}$	~NC with $k_{68} \simeq 0$ and $k^o_{78} \gg \kappa_{72},\kappa_{27}$ $I_{max} \simeq -FN\kappa_{27}$	18

Arrows (column 1) indicate change in Michaelis parameter with increasing negative voltage. NC = no change

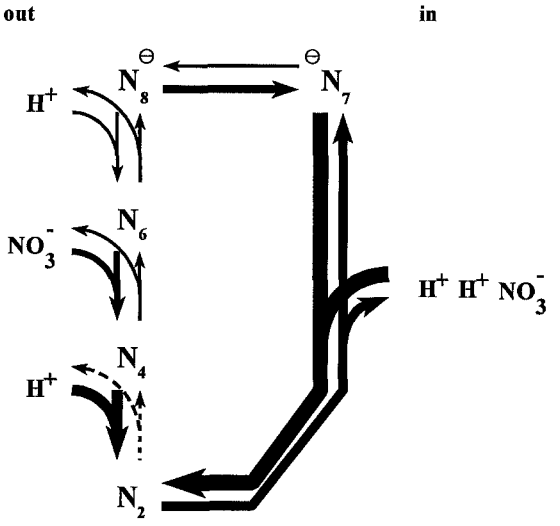

Fig. 12. Reaction kinetic cycle for *Arabidopsis* NO_3^- transporter. Line weights drawn to convey the relative magnitudes for the reaction constants. Key features are: (i) overall rate limitation in the forward (counter-clockwise) direction by membrane transit of the charged (unloaded) carrier (reaction constant k^o_{78}); (ii) rate dominance of the binding/debinding steps inside the cell, determined by the lumped constants κ_{27} and κ_{72}; (iii) kinetic isolation of NO_3^- binding outside from membrane charge transit. Details in the text.

Characteristics and Implications of the Model

A summary of Model II(M) and its characteristics are given schematically in Fig. 12. The relative size ordering of reaction constants is indicated by the weight of the arrows and highlights a number of prominent features as well as offering several experimentally testable predictions.

(i) Overall, the balance of rate-dominant to rate-limiting reaction steps is weighted in favor of the loaded (uncharged) carrier. In the forward (counter-clockwise) direction, membrane transit of the charged (unloaded) carrier is sufficiently slow to be rate-limiting at zero membrane voltage and, thus, bestows on the overall reaction cycle a strong voltage dependence over the entire physiological range (*see* Figs. 3 and 5). The voltage-dependent step, itself, is biased with the ratio $k^o_{78}/k^o_{87} < 1$, so that the carrier must be "drawn" across the membrane by depleting state N_8 through H^+ binding outside. This characteristic is a necessary consequence of the asymmetry in reaction flow in the cycle *vs.* that of charge movement. It also weights the carrier cycle in favor of a strong interaction between $[H^+]_o$ and membrane voltage (*see below*).

(ii) The lumped reaction constants κ_{72} and κ_{27}, that subsume NO_3^- and H^+ binding/debinding inside the cell, are among the fastest steps in the carrier cycle. The transition is biased somewhat to the bound state of the carrier and, as a consequence, NO_3^- transport is expected to show a sensitivity to ligand concentrations inside the cell. This prediction is consistent with observations that cytoplasmic acid loads significantly reduce the capacity for NO_3^- transport in induced cells (A. Meharg and M. Blatt, *manuscript in preparation*), and it may also implicate a role for cytoplasmic $[NO_3^-]$ in modulating the activity of the transport system (Ullrich, 1987).

(iii) NO_3^--binding, characterised by the reaction constant product $k^o_{64}[NO_3^-]_o$, is kinetically isolated from the voltage-dependent transition $N_7 \rightleftharpoons N_8$ by a single, slow H^+-binding step. It is this step that confers the profound pH_o-dependence to NO_3^- transport in *Arabidopsis* (Figs. 6–8), and it accounts for the correspondingly large negative slope and currents observed near zero and at positive clamp voltages in Figs. 3, 5 and 6; *see also* (Blatt, 1986). The placement of NO_3^- binding between the two H^+-binding steps, slow and fast, leads to the prediction that $[H^+]_o$ should have a significant effect on the K_m of the transporter for NO_3^-, but with little influence on the maximum transport rate because NO_3^--binding itself is a dominant fast reaction in the forward direction. These characteristics alone may account for the widely varying reports of the pH_o-sensitivity for NO_3^- transport (Rao & Rains, 1976; Doddema & Telkamp, 1979; Fuggi, 1985; Ullrich & Novacky, 1990), which have been based on measurements at a single $[NO_3^-]_o$ only. Finally, the apposition of H^+-binding with membrane charge transit and the dominant reaction constant $k^o_{81}e^{u/2}$ should give rise to an apparent equivalence between electrical and chemical ($[H^+]$) driving forces. Again, although not put to the test in the present study, such behavior has been described for a number of H^+-coupled or H^+ transporting electroenzymes, including the K^+-H^+ symporter of *Neurospora* (Blatt et al., 1987) and the H^+-ATPases of *Neurospora* [*see* (Hansen et al., 1981)] and *Chara* (Blatt et al., 1990). It has been ascribed to a "proton-conducting well" structure (Mitchell, 1969), nonetheless the behavior is readily accommodated within this simple reaction-kinetic scheme [*see* also (Hansen et al., 1981; Blatt et al., 1987; Blatt et al., 1990)].

One final point bears mentioning in relation to the effects of membrane voltage on NO_3^- transport activity. Although in principle voltage sensitivity is a common feature of all rheogenic transport processes, high-affinity NO_3^- transport—at least in *Arabidopsis*—is unusual amongst anion transporters as it is for H^+-coupled transport processes generally: its region of steep voltage dependence is situated within the normal range of physiological membrane potentials. In most other H^+-coupled systems known to date transport currents have appeared largely voltage-insensitive (Hansen & Slayman, 1978; Beilby & Walker, 1981; Felle, 1981; Sanders & Hansen, 1981; Sanders et al., 1983), consistent with equilibrium potentials situated well-positive of the normal range of membrane potentials [but see (Blatt, 1986)]. An important consequence for NO_3^- transport is that uptake of the

anion must be strongly influenced by factors which affect the prevailing membrane voltage. From Figs. 3–5 it is clear that shifting the membrane positive-going from −200 to −100 mV can reduce the NO_3^- current by 70–80% under constant $[NO_3^-]_o$ and pH_o. This behavior provides a simple, and quantitatively consistent explanation for the sensitivity of NO_3^- transport to metabolic inhibitors such as cyanide and azide (Rao & Rains, 1976; Schloemer & Garrett, 1974; Glass et al., 1990) which generally depolarize plant and fungal plasma membranes. Furthermore, the explanation may apply to the response of NO_3^- uptake to other transported solutes against which the transporter must "compete" for the electrical driving force. There are numerous reports that anions such as Cl^- (Ullrich & Novacky, 1990; Hawkins & Lewis, 1993) as well as nitrogenous compounds, including NH_4^+ (Goldsmith et al., 1973; Deane-Drummond, 1985; Henriksen et al., 1990; Henriksen & Spanswick, 1993), may interfere with NO_3^- transport or regulate its activity. Yet these solutes, equally, will draw on and depolarise the membrane potential, thereby reducing NO_3^- uptake—but by virtue of its inherent kinetic dependence on membrane voltage rather than any direct interaction with the NO_3^- transporter itself. Whether such an interpretation is justified now awaits experimental testing.

We are grateful to Tony Miller (Rothamsted) for helpful comments and critical reading of the manuscript. This work was aided by equipment grants from the Royal Society and the University of London Central Research Fund, and was supported by AFRC Research Grant PG32/530.

References

Beilby, M., Walker, N.A. 1981. Chloride transport in *Chara*. I: Kinetics and current-voltage curves for a probable proton symport. *J. Exptl. Bot.* **32:**43–54

Blatt, M.R. 1986. Interpretation of steady-state current-voltage curves: consequences and implications of current subtraction in transport studies. *J. Membrane Biol.* **92:**91–110

Blatt, M.R. 1987*a*. Electrical characteristics of stomatal guard cells: the ionic basis of the membrane potential and the consequence of potassium chloride leakage from microelectrodes. *Planta* **170:**272–287

Blatt, M.R. 1987*b*. Electrical characteristics of stomatal guard cells: the contribution of ATP-dependent, "electrogenic" transport revealed by current-voltage and different-current-voltage analysis. *J. Membrane Biol.* **98:**257–274

Blatt, M.R., Rodriguez-Navarro, A., Slayman, C.L. 1987. Potassium-proton symport in *Neurospora:* kinetic control by pH and membrane potential. *J. Membrane Biol.* **98:**169–189

Blatt, M.R., Beilby, M.J., Tester, M. 1990. Voltage dependence of the *Chara* proton pump revealed by current-voltage measurement during rapid metabolic blockade and cyanide. *J. Membrane Biol.* **114:**205–223

Blatt, M.R. 1991. A Primer in Plant Electrophysiological Methods. In: Methods in Plant Biochemistry, K. Hostettmann, editor. pp. 281–321, Academic Press, London

Blatt, M.R., Armstrong, F. 1993. K^+ channels of stomatal guard cells: abscisic acid-evoked control of the outward rectifier mediated by cytoplasmic pH. *Planta* **191:**330–341

Blatt, M.R., Slayman, C.L. 1983. KCl leakage from microelectrodes and its impact on the membrane parameters of a nonexcitable cell. *J. Membrane Biol.* **72:**223–234

Blatt, M.R., Slayman, C.L. 1987. Role of "active" potassium transport in the regulation of cytoplasmic pH by nonanimal cells. *Proc. Natl. Acad. Sci. USA* **84:**2737–2741

Bush, D.R. 1990. Electrogenicity, pH-dependence, and stoichiometry of the proton-sucrose symport. *Plant Physiol.* **93:**1590–1596

Clarkson, D.T., Saker, L.R., Purves, J.V. 1989. Depression of nitrate and ammonium transport in barley plants with diminished sulfate status—evidence of co-regulation of nitrogen and sulfate intake. *J. Exp. Bot.* **40:**953–963

Deanne-Drummond, C.E. 1985. Regulation of nitrate uptake in *Chara corallina* cells via NH4+ stimulation of NO3-efflux. *Plant Cell Environ.* **8:**105–110

Doddema, H., Hofstra, J.J., Feenstra, W.J. 1978. Uptake of nitrate by mutants of *Arabidopsis thaliana* disturbed in uptake or reduction of nitrate. I. Effect of nitrogen source during growth on uptake of nitrate and chlorate. *Physiol. Plant.* **43:**343–350

Doddema, H., Talkamp, G.P. 1979. Uptake of nitrate by mutants of *Arabidopsis thaliana,* disturbed in uptake or reduction of nitrate. II. Kinetics. *Physiol. Plant.* **45:**332–338

Eddy, A.A., Hopkins, P.G. 1985. The putative electrogenic nitrate-proton symport of the yeast *Candida utilis. Biophys. J.* **231:**291–297

Felle, H. 1981. Steriospecificity and electrogenicity of amino acid transport in *Riccia fluitans. Planta* **152:**505–512

Fuggi, A. 1985. Mechanism of proton-linked nitrate uptake by *Cyanidium caldarium,* and acidophilic non-vacuolated alga. *Biochim. Biophys. Acta* **815:**392–398

Glass, A.D.M., Siddiqui, M.Y., Ruth, T.J., Rufty, T.W.J. 1990. Studies of the uptake of nitrate in barley. *Plant Physiol.* **93:**1585–1589

Glass, A.D.M., Shaff, J.E., Kochian, L.V. 1992. Studies of the uptake of nitrate in barley. IV. Electrophysiology. *Plant Physiology* **99:**456–463

Goldsmith, J., Livoni, J.P., Norberg, C.L., Segel, I.H. 1973. Regulation of nitrate uptake in *Penicillium chrysogenum* by ammonium ion. *Plant Physiol.* **52:**362–367

Goyal, S.S., Huffaker, R.C. 1986. The uptake of NO_3^-, NO_2^-, and NO_4^+ by intact wheat (*Triticum aestivum*) seedlings. I. Induction and kinetics of transport systems. *Plant Physiol.* **82:**1051–1056

Gradmann, D., Kleiber, H.-G., Hansen, U.-P. 1987. Reaction kinetic parameters for ion transport from steady-state current-voltage curves. *Biophys. J.* **51:**569–585

Hansen, U.-P., Gradmann, D., Sanders, D., Slayman, C.L. 1981. Interpretation of current-voltage relationships for "active" ion transport systems: I. Steady-state reaction-kinetic analysis of class I mechanisms. *J. Membrane Biol.* **63:**165–190

Hansen, U.-P., Slayman, C.L. 1978. Current-voltage relationships for a clearly electrogenic cotransport system. In: Membrane Transport Processes. J.F. Hoffman, editor. pp. 141–154, Raven, New York

Hawkins, H.J., Lewis, O.A.M. 1993. Effect of NaCl salinity, nitrogen form, calcium and potassium concentration on nitrogen uptake and kinetics in *Triticum aestivum* l cv gamtoos. *New Phytologist* **124:**171–177

Heimer, Y.M., Filner, P. 1970. Regulation of the nitrate assimilation pathway in cultured tobacco cells: III. The nitrate uptake system. *Biochim. Biophys. Acta* **230:**362–372

Henriksen, G.H., Bloom, A.J., Spanswick, R.M. 1990. Measurement of net fluxes of ammonium and nitrate at the surface of barley roots using ion-selective microelectrodes. *Plant Physiol.* **93:**271–280

Henriksen, G.H., Spanswick, R.M. 1993. Investigation of the apparent induction of nitrate uptake in barley (*Hordeum vulgare* L.) using NO_3^--selective microelectrodes. *Plant Physiol.* **103:**885–892

Hodgkin, A.L., Huxley, A.F., Katz, B. 1952. Measurements of current-voltage relations in the membrane of the giant axon of *Loligo. J. Physiol.* **116:**424–448

Läuger, P. 1991. Electrogenic Ion Pumps. pp. 1–313. Sinauer Press, Sunderland, MA

Läuger, P., Stark, G. 1970. Kinetics of carrier-mediated ion transport across lipid bilayer membranes. *Biochim. Biophys. Acta* **211:**458–466

Li, Z.-C., Bush, D.R. 1990. .delta.pH-dependent amino acid transport in plasma membrane vesicles isolated from sugar beet leaves. *Plant Physiol.* **94:**268–277

MacKown, C.T. 1987. Nitrate uptake and assimilation following nitrate deprivation. *J. Exp. Bot.* **38:**1079–1090

Marquardt, D. 1963. An algorithm for fleast-squaires estimation of nonlinear parameters. *J. Soc. Ind. Appl. Math.* **11:**431–441

McClure, P.R., Kochian, L.V., Spanswick, R.M., Shaff, J.E. 1990. Evidence for cotransport of nitrate and protons in maize roots. 1. effects of nitrate on the membrane potential. *Plant Physiol.* **93:**281–289

McCulloch, S.R., Beilby, M.J., Walker, N.A. 1990. Transport of potassium in *Chara australis:* II. Kinetics of a symport with sodium. *J. Membrane Biol.* **115:**129–143

McCutcheon, S.L., Bown, A.W. 1987. Evidence for a specific glutamate/H^+ cotransport in isolated mesophyll cells. *Plant Physiol.* **83:**691–697

Meharg, A.A., Maurousett, L., Blatt, M.R. 1994. Cable correction of membrane currents recorded from root hairs of *Arabidopsis thaliana* L. *J. Exp. Bot.* **45:**1–6

Miller, A.J., Zhen, R.-G. 1991. Measurement of intracellular nitrate concentrations in *Chara* using nitrate-selective microelectrodes. *Planta* **184:**47–52

Mitchell, P. 1969. Chemiosmotic coupling and energy transduction. *Theor. Exp. Biophys.* **2:**159–216

Nelder, J.A., Mead, R. 1965. A simplex method for function minimization. *Comp. J.* **7:**308–313

Newman, I.A., Kochian, L.V., Grusak, M.A., Lucas, W.J. 1987. Fluxes of H^+ and K^+ in corn roots. *Plant Physiol.* **84:**1177–1184

Press, W., Flannerly, B., Teukolsky, S., Vetterling, W. 1986. *Numerical Recipies: The Art of Scientific Computing.* Cambridge University, Cambridge

Rao, K.P., Rains, D.W. 1976. Nitrate absorption by barley. I. Kinetics and energetics. *Plant Physiol.* **57:**55–58

Rodriguez-Navarro, A., Blatt, M.R., Slayman, C.L. 1986. A potassium-proton symport in *Neurospora crassa. J. Gen. Physiol.* **87:**649–674

Rufty, T.W., Jr., MacKown, C.T., Israel, D.W. 1990. Phosphorus stress effects on assimilation of nitrate. *Plant Physiol.* **94:**328–333

Salisbury, F., Ross, C. 1984. *Plant Physiology.* pp. 1–254. Wadsworth, Belmont, CA

Sanders, D., Slayman, C.L., Pall, M. 1983. Stoichiometry of H^+/amino-acid cotransport in *Neurospora crassa* revealed by current-voltage analysis. *Biochim. Biophys. Acta* **735:**67–76

Sanders, D., Hansen, U.-P., Gradmann, D., Slayman, C.L. 1984. Generalized kinetic analysis of ion-driven cotransport systems: a unified interpretation of selective ionic effects on Michaelis parameters. *J. Membrane Biol.* **77:**123–152

Sanders, D. 1990. Kinetic modeling of plant and fungal membrane transport systems. *Ann. Rev. Plant Physiol. Mol. Biol.* **41:**77–108

Sanders, D., Hansen, U.-P. 1981. Mechanism of Cl^- transport at the plasma membrane of *Chara corallina:* II. Transinhibition and determination of H^+/Cl^- binding order from a reaction kinetic model. *J. Membrane Biol.* **58:**139–153

Schloemer, R.H., Garrett, R.H. 1974. Nitrate transport system in *Neurospora crassa. J. Bacteriol.* **118:**259–269

Schwab, W., Komor, E. 1978. A possible mechanistic role of the membrane potential in proton-sugar cotransport of *Chlorella. FEBS Lett* **87:**157–160

Segel, I.H. 1993. Enzyme Kinetics. pp. 1–957. Wiley Interscience, New York

Tischner, R., Waldeck, B., Goyal, S.S., Rains, W.D. 1993. Effect of nitrate pulses on the nitrate-uptake rate, synthesis of mRNA coding for nitrate reductase, and nitrate-reductase activity in roots of barley seedlings. *Planta* **189:**533–537

Ullrich, C.I., Novacky, A.J. 1990. Extracellular and intracellular pH and membrane-potential changes induced by K^+, Cl^-, $H_2PO_4^-$, and NO_3^- uptake and fusicoccin in root hairs of *Limnobium stoloniferum. Plant Physiology* **94:**1561–1567

Ullrich, W.R., Larsson, M., Larsson, C.-M., Lesch, S., Novacky, A. 1984. Ammonium uptake in *Lemna gibba* G1, related membrane potential changes, and inhibition of anion uptake. *Plant Physiol.* **61:**369–376

Ullrich, W.R. 1987. Nitrate and ammonium uptake in green algae and higher plants: mechanisms and relationship with nitrate metabolism. *In:* Inorganic Nitrogen Metabolism, W.R. Ullrich, editor. pp. 32–41, Springer Verlag, Berlin

Ullrich, W.R., Novacky, A. 1981. Nitrate-dependent membrane potential changes and their induction in *Lemna gibba* G1. *Plant Sci. Lett.* **22:**211–217

Zhen, R.-G., Koyro, H.-W., Leigh, R.A., Tomos, A.D., Miller, A.J. 1991. Compartmental nitrate concentrations in barley root cells measured with nitrate-selective microelectrodes and by single-cell sap sampling. *Planta* **185:**356–361